CHEMISTRY
A EUROPEAN JOURNAL

DOI: 10.1002/chem.200700715

Self-Assemblies Based on $[Cp_2Mo_2(CO)_4(\mu,\eta^2\text{-}P_2)]$—Solid-State Structure and Dynamic Behaviour in Solution

Manfred Scheer,*[a] Laurence J. Gregoriades,[a, b] Manfred Zabel,[a] Junfeng Bai,[a, c] Ingo Krossing,*[d] Gunther Brunklaus,[e, f] and Hellmut Eckert*[e]

Dedicated to Professor Vladimir E. Fedorov on the occasion of his 70th birthday

Abstract: Reaction of complex $[Cp_2Mo_2(CO)_4(\mu,\eta^2\text{-}P_2)]$ ($Cp = C_5H_5$ (**1**)) with $CuPF_6$, AgX ($X = BF_4$, ClO_4, PF_6, SbF_6, $Al\{OC(CF_3)_3\}_4$) and $[(Ph_3P)Au(THF)][PF_6]$ (THF = tetrahydrofuran), respectively, results in the facile formation of the dimers **3b**–**h** of the general formula $[M_2(\{Cp_2Mo_2(CO)_4(\mu,\eta^2:\eta^2\text{-}P_2)\}_2)(\{Cp_2Mo_2(CO)_4(\mu,\eta^2:\eta^1:\eta^1\text{-}P_2)\}_2)][X]_2$ (M = Cu, Ag, Au; $X = BF_4$, ClO_4, PF_6, SbF_6, $Al\{OC(CF_3)_3\}_4$). As revealed by X-ray crystallography, all these dimers comprise dicationic moieties that are well-separated from the weakly coordinating anions in the solid state. If **1** is allowed to react with $AgNO_2$ and LAuCl (L = CO or tetrahydrothiophene), respectively, the dimer $[Ag_2\{Cp_2Mo_2(CO)_4(\mu,\eta^2:\eta^1:\eta^1\text{-}P_2)\}_2(\eta^2\text{-}NO_2)_2]$ (**5**) and the complex $[AuCl\{Cp_2Mo_2(CO)_4(\mu,\eta^2:\eta^1\text{-}P_2)\}]$ (**6**) are formed, which have also been characterised by X-ray crystallography. In compounds **5** and **6**, the anions remain coordinated to the Group 11 metal centres. Spectroscopic data suggest that the dimers **3b**–**h** display dynamic behaviour in solution and this is discussed by using the comprehensive results obtained for **3g** (M = Ag; $X = Al\{OC(CF_3)_3\}_4$) as a basis. The interpretation of the experimental results is facilitated by density functional theory (DFT) calculations on **3g** (structures, energetics, NMR shielding tensors). The ^{31}P magic angle spinning (MAS) NMR spectra recorded for the dimers **3b** (M = Cu; $X = PF_6$) and **3c** (M = Ag; $X = BF_4$) as well as that of the previously reported one-dimensional (1D) polymer $[Ag_2\{Cp_2Mo_2(CO)_4(\mu,\eta^2:\eta^1:\eta^1\text{-}P_2)\}_3(\mu,\eta^1:\eta^1\text{-}NO_3)]_n[NO_3]_n$ (**4**) are also discussed herein and the strong dependence of the chemical shift of the phosphorus atoms within each compound on subtle structural differences in the solid state is demonstrated. Furthermore, the X-ray crystallographic and ^{31}P MAS NMR spectroscopic characterisation of a new polymorph of **1** is reported.

Keywords: density functional calculations · group 11 metals · molybdenum · NMR spectroscopy · phosphorus

Introduction

The self-organisation of discrete units to form supramolecular aggregates and networks is a field at the vanguard of current chemical research.[1] In contrast to typical approaches in this area, in which nitrogen-, oxygen- and/or sulphur-donor-containing organic ligands are employed to con-

[a] Prof. Dr. M. Scheer, Dr. L. J. Gregoriades, Dr. M. Zabel, Prof. Dr. J. Bai
Institut für Anorganische Chemie der Universität Regensburg, 93040 Regensburg (Germany)
Fax: (+49) 941-943-4439
E-mail: manfred.scheer@chemie.uni-regensburg.de

[b] Dr. L. J. Gregoriades
Present address:
Institut für Chemie der Humboldt-Universität zu Berlin 10099 Berlin (Germany)

[c] Prof. Dr. J. Bai
Present address:
Coordination Chemistry Institute and the State Key Laboratory of Coordination Chemistry, Nanjing University, 210093 Nanjing (China)

[d] Prof. Dr. I. Krossing
Institut für Anorganische und Analytische Chemie der Albert-Ludwigs-Universität Freiburg, 79104 Freiburg (Germany)
Fax: (+49) 761-203-6001
E-mail: krossing@uni-freiburg.de

[e] Dr. G. Brunklaus, Prof. Dr. H. Eckert
Institut für Physikalische Chemie der Westfälischen Wilhelms-Universität, Münster, 48149 Münster (Germany)
Fax: (+49) 251-83-29159
E-mail: eckerth@uni-muenster.de

[f] Dr. G. Brunklaus
Present address:
Max-Planck-Institut für Polymerforschung, D-55128 Mainz (Germany)

nect different metal centres, the novelty of our work lies in the use of organometallic E_n-[2] and E_mS_n-ligand[3] complexes (E = P, As) as connecting moieties. One of the P_n-ligand complexes utilised in our group as a linking unit between metal centres is the tetrahedrane complex $[Cp_2Mo_2(CO)_4(\mu,\eta^2\text{-}P_2)]$ (Cp = C_5H_5 (**1**)).[4] The reaction of **1** with Cu^I halides leads to the formation of the one-dimensional (1D) polymers $[Cu(\mu\text{-}X)\{Cp_2Mo_2(CO)_4(\mu,\eta^2{:}\eta^1{:}\eta^1\text{-}P_2)\}]_n$ (X = Cl (**2a**), Br (**2b**), I (**2c**)).[2a,d] $Ag[CF_3SO_3]$ reacts with **1** to yield the oligomeric dicationic species $[Ag_2(\{Cp_2Mo_2(CO)_4(\mu,\eta^2{:}\eta^2\text{-}P_2)\}_2)(\{Cp_2Mo_2(CO)_4(\mu,\eta^2{:}\eta^1{:}\eta^1\text{-}P_2)\}_2)][CF_3SO_3]_2$ (**3a**), whereas the reaction of **1** with $AgNO_3$ results in the undulated 1D polymer $[Ag_2\{Cp_2Mo_2(CO)_4(\mu,\eta^2{:}\eta^1{:}\eta^1\text{-}P_2)\}_3(\mu,\eta^1{:}\eta^1\text{-}NO_3)]_n[NO_3]_n$ (**4**).[2a] We report herein the synthesis, solid-state structures and spectroscopic characterisation of the dimers **3b–h** of the general formula $[M_2(\{Cp_2Mo_2(CO)_4(\mu,\eta^2{:}\eta^2\text{-}P_2)\}_2)(\{Cp_2Mo_2(CO)_4(\mu,\eta^2{:}\eta^1{:}\eta^1\text{-}P_2)\}_2)][X]_2$ (M = Cu, Ag, Au; X = BF_4, ClO_4, PF_6, SbF_6, $Al\{OC(CF_3)_3\}_4$), the dimer $[Ag_2\{Cp_2Mo_2(CO)_4(\mu,\eta^2{:}\eta^1{:}\eta^1\text{-}P_2)\}_2(\eta^2\text{-}NO_2)_2]$ (**5**) and the complex $[AuCl\{Cp_2Mo_2(CO)_4(\mu,\eta^2{:}\eta^1\text{-}P_2)\}]$ (**6**). Spectroscopic data suggest that the dimers **3a–h** display dynamic behaviour in solution in the form of monomer/dimer equilibria and the discussion of these equilibria draws upon the comprehensive analytical data obtained for **3g** (M = Ag; X = $Al\{OC(CF_3)_3\}_4$), owing to its superior solubility characteristics. Density functional theory (DFT) calculations on **3g** contribute to the elucidation of this unexpected dynamic behaviour. The results of the ^{31}P magic angle spinning (MAS) NMR spectroscopic investigation of the dimers **3b** (M = Cu; X = PF_6) and **3c** (M = Ag; X = BF_4) and the polymer **4** reveal that the chemical shift of the phosphorus atoms within each compound is strongly dependent on subtle conformational differences in the solid state.

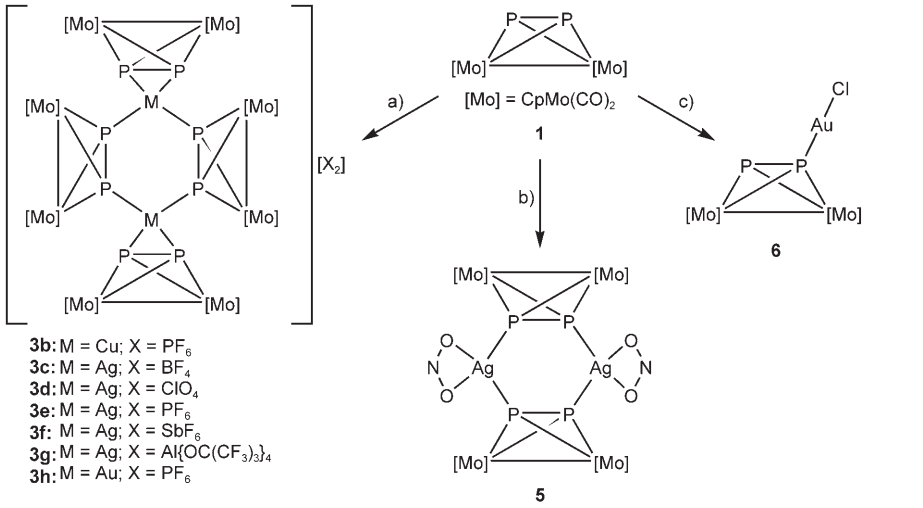

Scheme 1. Preparation of **3b–h**, **5** and **6**. a) $CuPF_6$, AgX (X = BF_4, ClO_4, PF_6, SbF_6, $Al\{OC(CF_3)_3\}_4$) or $[(Ph_3P)Au(THF)][PF_6]$; CH_3CN, CH_2Cl_2, CH_3CN/CH_2Cl_2, CH_2Cl_2/THF or CH_2Cl_2/toluene; room temperature; b) $AgNO_2$; CH_3CN or CH_3CN/CH_2Cl_2; room temperature; c) LAuCl (L = CO or tetrahydrothiophene (THT)); CH_2Cl_2 or CH_2Cl_2/toluene; low temperature (see Experimental Section; L = CO), room temperature (L = THT).

Results and Discussion

Synthesis of the products: The dimers **3b–h** are easily prepared at room temperature in moderate to high yield by the reaction of complex **1** with $CuPF_6$, AgX (X = BF_4, ClO_4, PF_6, SbF_6, $Al\{OC(CF_3)_3\}_4$) and $[(Ph_3P)Au(THF)][PF_6]$ (THF = tetrahydrofuran), respectively, in a 2:1 stoichiometry (Scheme 1). The $[Al\{OC(CF_3)_3\}_4]^-$ ion was employed as one of the weakly coordinating anions (WCAs) in order to enhance the solubility of the resulting product **3g** and thus, permit its comprehensive spectroscopic characterisation in solution. Compounds **3b–h** are air- and light-sensitive, red-orange to ruby-red crystalline solids, but can be stored indefinitely under an inert atmosphere at ambient conditions. With the exception of **3g**, these dimers are only sparingly soluble in polar solvents such as CH_3CN. In contrast, complex **3g** is readily soluble in CH_2Cl_2, THF and CH_3CN, and moderately soluble in toluene.

The dependence of the composition of the product on reactant stoichiometry was studied by using the complex **1**/$Ag[Al\{OC(CF_3)_3\}_4]$ system and it could be shown that the 2:1 dimer **3g** is always formed regardless of the reactant stoichiometry used (1:1, 2:1 or 6:1), which suggests that the 2:1 product represents a thermodynamic minimum for this system.

The reaction of **1** with $AgNO_2$ in CH_3CN or a mixture of CH_3CN and CH_2Cl_2 at room temperature leads to the dimer **5** as an insoluble air- and light-sensitive dark brown microcrystalline powder (Scheme 1). Complex **5** can be stored indefinitely under an inert atmosphere at ambient conditions. As demonstrated for **3g**, the formation of **5** also appears to be independent of reactant stoichiometry. Compound **5** is obtained regardless of whether a 1:1 or 2:1 reactant stoichiometry is employed. The formation of the dimer **5** was unexpected since the reaction of **1** with $AgNO_3$ yields the 1D polymer **4**, in which half of the nitrate ions are incorporated in the polymer chain as bridging ligands.

Complex **6** can be prepared by the reaction of **1** with [LAuCl] (L = CO,[5] tetrahydrothiophene (THT)[6]) in a 1:1 stoichiometry in CH_2Cl_2 or a mixture of CH_2Cl_2 and toluene, at room temperature (L = THT) and at low temperature (L = CO), respectively (Scheme 1 and Experimental Section). Compound **6** is an air-sensitive, red-orange microcrystalline powder, which is only sparingly soluble in solvents

such as CH_2Cl_2 and THF, and can be stored indefinitely under an inert atmosphere at ambient conditions. Experiments in which **1** and [LAuCl] were allowed to react in a stoichiometric ratio of 1:2 resulted, nevertheless, in the formation of the 1:1 product **6**.

X-ray crystallographic characterisation: A new polymorph of the starting material **1**, crystallised from a 1:1 mixture of CH_3CN and CH_2Cl_2, as well as the compounds **3b–h**, **5** and **6** have all been characterised by single crystal X-ray crystallography and the measurement details are summarised in Tables 1–3. A section of the crystal lattice of the new polymorph of **1**, viewed along the crystallographic *c* axis, is de-

Table 1. Crystallographic data of the new polymorph of **1** and the products **3b–d**.

Crystallographic Data	**1**	**3b**·2 CH_2Cl_2	**3c**·6 CH_3CN	**3d**·2 CH_3CN
empirical formula	$C_{14}H_{10}Mo_2O_4P_2$	$C_{58}H_{44}Cl_4Cu_2F_{12}Mo_8O_{16}P_{10}$	$C_{68}H_{58}Ag_2B_2F_8Mo_8N_6O_{16}P_8$	$C_{60}H_{46}Ag_2Cl_2N_2Mo_8O_{24}P_8$
M_r	496.04	2571.04	2619.84	2481.20
crystal size [mm]	0.07×0.05×0.04	0.20×0.20×0.05	0.30×0.16×0.04	0.26×0.10×0.04
T [K]	103(2)	200(1)	203(2)	123(1)
λ [Å]	1.54178	0.71073	0.56087	0.71073
crystal system	monoclinic	triclinic	triclinic	triclinic
space group	$P2_1/c$	$P\bar{1}$	$P\bar{1}$	$P\bar{1}$
a [Å]	17.056(8)	13.033(3)	11.843(2)	12.006(2)
b [Å]	7.568(2)	13.776(3)	13.479(3)	13.484(1)
c [Å]	12.735(5)	15.031(3)	15.542(3)	15.538(2)
α [°]	90	80.50(3)	115.03(3)	114.39(1)
β [°]	107.84(4)	64.92(3)	100.09(3)	100.88(1)
γ [°]	90	64.45(3)	95.27(3)	95.61(1)
V [Å^3]	1565(1)	2204.8(8)	2174.5(8)	2205.8(5)
Z	4	1	1	1
ρ_{calcd} [g cm^{-3}]	2.105	1.936	2.001	1.868
μ [mm^{-1}]	15.194	1.950	4.590	1.800
θ range [°]	6.45–50.95	2.20–25.99	1.95–20.00	2.00–25.80
reflections collected/unique	5212/1662	13893/8015	13892/7897	19958/7892
obsvd reflns with [$I>2\sigma(I)$]	1272	5980	5661	6821
R_{int}	0.0317	0.0313	0.0547	0.0256
GOF on F^2	0.924	1.028	1.014	1.041
final R indices [$I>2\sigma(I)$]	$R_1=0.0259$ $wR_2=0.0487$	$R_1=0.0511$ $wR_2=0.1434$	$R_1=0.0507$ $wR_2=0.1188$	$R_1=0.0280$ $wR_2=0.0789$
R indices (all data)	$R_1=0.0382$ $wR_2=0.0498$	$R_1=0.0643$ $wR_2=0.1486$	$R_1=0.0797$ $wR_2=0.1331$	$R_1=0.0327$ $wR_2=0.0806$
max/min $\Delta\rho$ [e Å^{-3}]	0.556/−0.462	2.517/−0.524	1.297/−1.030	1.356/−0.777

Table 2. Crystallographic data of the products **3e–g**.

Crystallographic Data	**3e**·2 CH_3CN	**3f**·4.5 CH_3CN	**3g**·CH_2Cl_2
empirical formula	$C_{60}H_{46}Ag_2F_{12}N_2Mo_8O_{16}P_{10}$	$C_{65}H_{53.5}Ag_2F_{12}N_{4.5}Mo_8O_{16}P_8Sb_2$	$C_{89}H_{42}Ag_2Al_2Cl_2F_{72}Mo_8O_{24}P_8$
M_r	2571.95	2844.14	4219.10
crystal size [mm]	0.40×0.32×0.22	0.32×0.15×0.10	0.30×0.20×0.10
T [K]	173(1)	173(1)	150(1)
λ [Å]	0.71073	0.71073	0.71073
crystal system	triclinic	triclinic	triclinic
space group	$P\bar{1}$	$P\bar{1}$	$P\bar{1}$
a [Å]	12.193(1)	12.112(1)	13.838(3)
b [Å]	13.420(1)	13.733(1)	14.597(3)
c [Å]	15.392(2)	15.671(1)	18.576(4)
α [°]	112.96(1)	113.73(1)	105.90(3)
β [°]	100.11(1)	99.30(1)	100.30(3)
γ [°]	94.27(1)	93.50(1)	111.27(3)
V [Å^3]	2254.5(5)	2332.0(4)	3197(1)
Z	1	1	1
ρ_{calcd} [g cm^{-3}]	1.894	2.025	2.192
μ [mm^{-1}]	1.753	2.231	1.381
θ range [°]	2.20–25.87	2.01–25.81	1.61–27.14
reflections collected/unique	31811/8068	20232/8344	22151/12619
obsvd reflns with [$I>2\sigma(I)$]	7528	6385	11722
R_{int}	0.0242	0.0286	0.0385
GOF on F^2	1.103	0.916	1.029
final R indices [$I>2\sigma(I)$]	$R_1=0.0283$ $wR_2=0.0864$	$R_1=0.0280$ $wR_2=0.0708$	$R_1=0.0348$ $wR_2=0.0937$
R indices (all data)	$R_1=0.0304$ $wR_2=0.0877$	$R_1=0.0392$ $wR_2=0.0731$	$R_1=0.0372$ $wR_2=0.0958$
max/min $\Delta\rho$ [e Å^{-3}]	1.224/−0.499	0.940/−0.649	0.690/−0.998

Table 3. Crystallographic data of the products **3h**, **5** and **6**.

Crystallographic Data	**3h**·2 C_4H_8O·2 CH_2Cl_2	**5**	**6**
empirical formula	$C_{66}H_{58}Au_2Cl_4F_{12}Mo_8O_{18}P_{10}$	$C_{28}H_{20}Ag_2Mo_4N_2O_{12}P_4$	$C_{14}H_{10}AuClMo_2O_4P_2$
M_r	2980.09	1299.84	728.46
crystal size [mm]	0.22×0.18×0.16	0.12×0.08×0.06	0.15×0.08×0.04
T [K]	173(1)	173(1)	203(1)
λ [Å]	0.71073	0.71073	0.56087
crystal system	triclinic	monoclinic	monoclinic
space group	$P\bar{1}$	$P2_1/c$	$P2_1/n$
a [Å]	13.156(1)	9.982(1)	8.345(2)
b [Å]	13.930(1)	10.552(1)	23.468(5)
c [Å]	15.215(1)	17.578(2)	9.278(2)
α [°]	78.52(1)	90	90
β [°]	64.62(1)	100.97(1)	103.03(3)
γ [°]	64.41(1)	90	90
V [Å^3]	2271.8(5)	1817.7(3)	1770.2(7)
Z	1	2	4
ρ_{calcd} [g cm^{-3}]	2.178	2.375	2.733
μ [mm^{-1}]	4.658	2.632	9.905
θ range [°]	2.79–25.93	2.26–27.98	1.91–20.79
reflections collected/unique	25284/8216	21303/4346	10844/3583
obsvd reflns with [$I>2\sigma(I)$]	5655	3528	2614
R_{int}	0.0489	0.0455	0.1520
GOF on F^2	0.920	0.978	1.128
final R indices [$I>2\sigma(I)$]	R_1=0.0455 wR_2=0.1071	R_1=0.0236 wR_2=0.0566	R_1=0.1017 wR_2=0.2568
R indices (all data)	R_1=0.0686 wR_2=0.1131	R_1=0.0325 wR_2=0.0581	R_1=0.1264 wR_2=0.2808
max/min $\Delta\rho$ [e Å^{-3}]	1.593/−0.854	0.987/−0.588	8.308/−4.984

picted in Figure 1. Unlike the polymorph of **1** reported originally,[4a] which contains two phosphorus atoms rendered equivalent by a C_2 axis bisecting the P–P bond, the new polymorph of **1** contains two crystallographically distinct phosphorus atoms. This is most likely attributable to packing effects induced by the solvent system employed in our work, since the original polymorph was crystallised from heptane. Nevertheless, the structural parameters of the new polymorph of **1** (Figure 1) are comparable to those of the original polymorph.[4a]

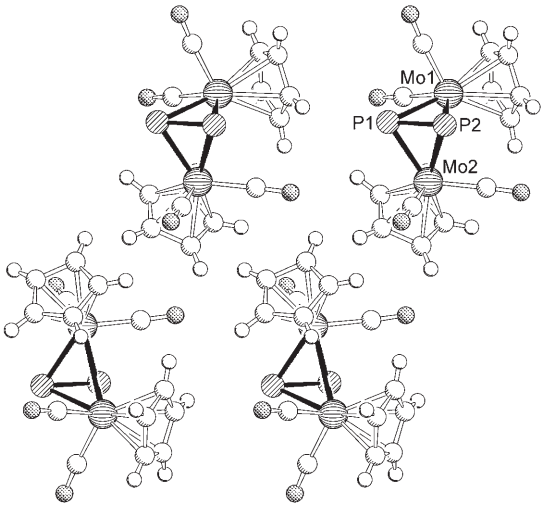

Figure 1. Section of the crystal lattice of the new polymorph of **1**, viewed along the crystallographic c axis. Selected bond lengths [Å] and angles [°]: P1–P2 2.080(2), Mo1–Mo2 3.036(2), P1–Mo1 2.554(2), P1–Mo2 2.472(2), P2–Mo1 2.472(2), P2–Mo2 2.548(2), Mo1-P1-Mo2 74.32(5), Mo1-P2-Mo2 74.43(5), P1-Mo1-Mo2 51.61(4), P1-Mo2-Mo1 54.06(4), P2-Mo1-Mo2 53.92(5), P2-Mo2-Mo1 51.64(4), P1-Mo1-P2 48.88(5), P1-Mo2-P2 48.94(5).

Compounds **3b–h** are structurally similar to the previously synthesised silver complex **3a**,[2a] in that they consist of a dication well-separated from the anions. In each dication, two metal centres M (M = Cu, Ag, Au) are doubly bridged by two units of **1**. Two further units of **1**, one per M centre, are attached in a side-on coordination mode and hence the coordination geometry about the M centres is pseudotetrahedral. The structure of the dication in the gold derivative **3h** is shown in Figure 2 and selected bond lengths and angles of the compounds **3b–h** are compared with those of **3a** in Table 4.

Compared to the P–P bond length in uncoordinated **1** (2.079(2),[4a] 2.080(2) Å[7]), the P–P bond lengths of the bridging units of **1** in complexes **3a**,**c–h** are somewhat

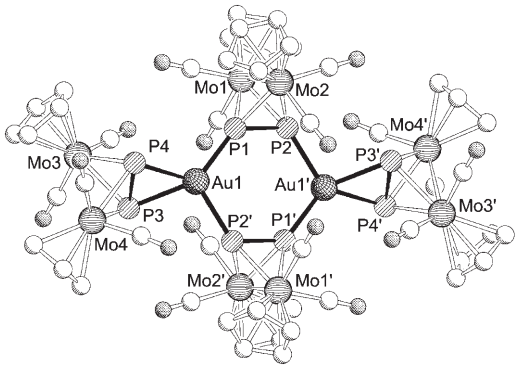

Figure 2. Structure of the dication in **3h** (hydrogen atoms omitted for clarity). For selected bond lengths and angles, see Table 4.

Table 4. Selected bond lengths [Å] and angles [°] of the dimers **3a–h**.

Dimer	**3a**[2a]	**3b**	**3c**	**3d**	**3e**	**3f**	**3g**	**3h**
M	Ag	Cu	Ag	Ag	Ag	Ag	Ag	Au
X	CF_3SO_3	PF_6	BF_4	ClO_4	PF_6	SbF_6	$Al\{OC(CF_3)_3\}_4$	PF_6
P_b–P_b[a]	2.098(2)	2.077(2)	2.096(3)	2.104(2)	2.099(1)	2.097(2)	2.091(1)	2.089(3)
P_s–P_s[a]	2.137(2)	2.149(2)	2.136(3)	2.150(1)	2.145(1)	2.133(2)	2.143(1)	2.186(3)
M–P_b	2.470(1)	2.259(2)	2.468(2)	2.476(1)	2.483(1)	2.481(1)	2.474(1)	2.349(3)
	2.489(1)	2.277(2)	2.487(2)	2.489(1)	2.485(1)	2.502(1)	2.478(1)	2.437(3)
M–P_s	2.610(1)	2.358(2)	2.606(2)	2.621(1)	2.620(1)	2.600(1)	2.580(1)	2.509(3)
	2.727(2)	2.378(2)	2.699(2)	2.676(1)	2.704(1)	2.774(1)	2.685(1)	2.536(3)
P_b-M-P_b	120.28(8)	111.37(8)	120.28(8)	120.50(4)	119.95(3)	118.89(4)	112.63(3)	111.15(9)
P_s-M-P_s	47.45(7)	53.97(6)	47.46(7)	47.87(3)	47.50(3)	46.63(4)	47.99(3)	51.36(8)
P_b-M-P_s	98.96(8)	102.89(7)	98.95(7)	100.30(3)	99.48(3)	97.99(4)	107.88(3)	99.74(9)
	108.32(8)	110.56(8)	108.34(7)	106.80(4)	106.98(3)	111.39(4)	109.28(4)	113.65(8)
	130.25(8)	133.70(7)	130.28(8)	131.07(4)	132.18(3)	129.05(4)	133.42(3)	131.44(8)
	131.04(8)	137.55(7)	131.01(7)	131.68(3)	132.73(4)	134.00(4)	134.43(3)	142.13(10)

P_b = P atom of bridging unit of **1**; P_s = P atom of side-on coordinated unit of **1**. [a] P–P bond length in uncoordinated **1** = 2.079(2),[4a] 2.080(2) Å.[7]

longer whereas these bond lengths in **3b** are essentially unchanged. In contrast, the P–P bond lengths of the side-on coordinated units of **1** are significantly longer in all dimers. In the dimer **3b**, the Cu–P_s (P_s = P atom of side-on coordinated unit of **1**) and the Cu–P_b (P_b = P atom of bridging unit of **1**) bond lengths are markedly shorter than the Cu–P bond lengths in reported $[Cu(PPh_3)_4]^+$ salts (2.465(2)–2.61(1) Å).[8] The Ag–P_s bond lengths in the complexes **3c–g** are comparable with the Ag–P bond lengths found in reported $[Ag(PPh_3)_4]^+$ salts (2.631(5)–2.746(5) Å),[8,9] whereas the Ag–P_b bond lengths are noticeably shorter. The Au–P bond lengths in the dication of **3h** compare well with those of $[\{(tppme)M'(\eta^3\text{-}P_3)\}_2Au]^+$ (tppme = $CH_3C(CH_2PPh_2)_3$; M′ = Co, Rh, Ir; 2.39(1)–2.54(1) Å),[10] $[Au(PPh_3)_4][BPh_4]$ (2.392(4)–2.610(9) Å)[11] and $[Au(Ph_2PCH_2CH_2PPh_2)_2Cl\cdot 2H_2O]$ (2.384(2)–2.412(2) Å).[12]

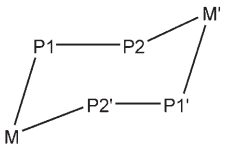

Figure 3. Schematic representation of the folded cores of the dications in **3a–h** with labelling scheme (M = Cu, Ag, Au).

The cores of the dications in **3a–h** comprise six-membered M_2P_4 rings (Figure 3) in a slight chair-conformation. The sizes of the folding angles of the M_2P_4 rings (dihedral angle between MP1P2′ and P1P2P1′P2′ planes, see Figure 3) are listed in Table 5 along with the radii of the corresponding anions.[13] The values of the silver derivatives **3a**,**c–g** reveal that the folding angle increases with anion size, a phenomenon most likely attributable to crystal packing effects. In contrast, no trend is apparent upon inspection of the folding angles of the PF_6^- derivatives **3b**,**e**,**h** and the size of the M^+ cations.

Table 5. Comparison of the anionic radii [Å] and folding angles [°] of the M_2P_4 rings (dihedral angle between MP1P2′ and P1P2P1′P2′ planes, see Figure 3) in compounds **3a–h**.

Compound	M	Anion	Anion radius	Folding angle
3b	Cu	PF_6^-	2.42	12.88(3)
3c	Ag	BF_4^-	2.05	6.05(3)
3d	Ag	ClO_4^-	2.25	6.74(3)
3a[2a]	Ag	$CF_3SO_3^-$	2.30	7.08(2)
3e	Ag	PF_6^-	2.42	7.96(3)
3f	Ag	SbF_6^-	2.52	10.11(5)
3g	Ag	$Al\{OC(CF_3)_3\}_4^-$	6.25	20.69(2)
3h	Au	PF_6^-	2.42	17.30(1)

The structure of dimer **5** is illustrated in Figure 4 and consists of two $AgNO_2$ moieties doubly bridged by two units of **1**. Thus, the coordination geometry about each Ag^I centre is pseudotetrahedral. The structure of **5** bears some resemblance to that of the dimers **3a–h** in that its core consists of a six-membered Ag_2P_4 ring in a chair-conformation (dihedral angle between Ag1P1P2′ and P1P2P1′P2′ planes = 24.91(1)°). The P–P bond lengths of the units of **1** in **5** (2.110(1) Å) are appreciably longer than that in uncoordinated **1** (2.079(2)[4a] and 2.080(2) Å[7]). The Ag–P bond lengths (2.417(8) and 2.560(8) Å) lie within and above the range defined by those of the complexes $[(AgNO_2)_m\text{-}(R_2P(R')PR_2)]_n$ (R = Ph, R′ = CH_2 (m = 1, n = 2); R = Ph, R′ = $(CH_2)_3$ (m = 1, n = 2); R = Ph, R′ = CH-CH (m = 2, n = 2); R = *para*-tolyl, R′ = (R)-(+)-1,1-binaphthyl (m = 1, n = 1)) (2.365(1)–2.490(2) Å).[14] The O-Ag-O angle (51.6(1)°) is

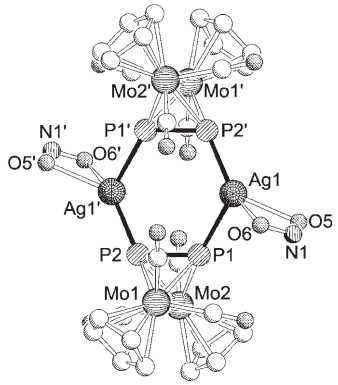

Figure 4. Structure of compound **5** (hydrogen atoms omitted for clarity). Selected bond lengths [Å] and angles [°]: P1–P2 2.110(1), Mo1–Mo2 3.046(1), Ag1–P1 2.560(8), Ag1–P2′ 2.417(8), Ag1–O5 2.439(3), Ag1–O6 2.379(3), P1-Ag1-P2′ 118.58(3), O5-Ag1-O6 51.6(1), P1-Ag1-O5 96.9(1), P1-Ag1-O6 94.71(8), P2′-Ag1-O5 136.30(9), P2′-Ag1-O6 138.71(7).

within the range defined by the reference compounds (41.0(5)–54.2(5)°).

The structure of **6** consists of a unit of **1** with the Lewis-acidic fragment [AuCl] coordinated to one of the P atoms (Figure 5). The P–P bond length (2.095(8) Å) is only slightly longer than that in the uncoordinated complex **1** (2.079(2),[4a] 2.080(2) Å[7]). The Au–P bond length (2.235(5) Å) compares well with that found in [(Ph$_3$P)AuCl][15] (2.232(1) Å), whereas the Au–Cl bond length (2.325(5) Å) is noticeably longer than that in the reference compound (2.277(1) Å). Although the coordination mode of the Au^{I} centre in [(Ph$_3$P)AuCl] is essentially linear (P-Au-Cl 179.7(1)°), the P-Au-Cl angle in **6** deviates appreciably from linearity (170.4(2)°).

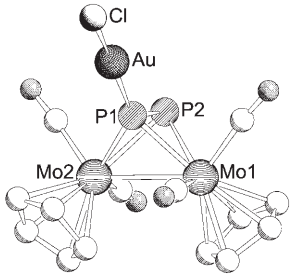

Figure 5. Structure of the compound **6** (hydrogen atoms omitted for clarity). Selected bond lengths [Å] and angles [°]: P1–P2 2.095(8), Mo1–Mo2 3.063(1), Au–P1 2.235(5), Au–Cl 2.325(5), P1-Au-Cl 170.4(2).

Solution spectroscopic data of the products: The ^{31}P{^{1}H} NMR spectra of the compounds **3a–h** in solution (**3a–g**: CD_3CN; **3h**: CD_2Cl_2) display slightly broad singlets[16] at room temperature which are shifted by about 25–35 ppm upfield compared to uncoordinated **1** (−43 ppm in CD_3CN), without any detectable coupling to the $^{107/109}$Ag or $^{63/65}$Cu nuclei (Table 6). Considering the solid-state structures of these compounds, one would expect at least two signals in the ^{31}P NMR spectra if the integrity of the corresponding dications were maintained in solution. However, the experimental spectra suggest dynamic behaviour in solution, which could not be resolved in previous investigations on **3a**.[2a]

Table 6. Room temperature ^{31}P{^{1}H} NMR chemical shifts of the compounds **3a–h** in solution (**3a–g**: CD_3CN; **3h**: CD_2Cl_2).

Compound	δ [ppm]	Compound	δ [ppm]
3a[2a]	−69.0	**3e**	−64.2
3b	−49.6	**3f**	−71.3
3c	−71.3	**3g**	−77.5
3d	−59.5	**3h**	−52.7

Positive ion electrospray ionisation mass spectrometry (ESI MS) measurements on the compounds **3c–g** in CH_3CN at room temperature reveal that the peaks with 100% relative abundance correspond to the monocation [Ag{Cp$_2$Mo$_2$(CO)$_4$P$_2$}$_2$]$^+$ (**I**). Other larger fragments, detected in smaller amounts, allude to the presence of the dication [Ag$_2${Cp$_2$Mo$_2$(CO)$_4$P$_2$}$_4$]$^{2+}$ (**II**) observed in the solid state and thus, to the existence of a dynamic monomer/dimer equilibrium in solution. In the case of **3e**, the ESI MS spectra even suggest the presence of the trication [Ag$_3${Cp$_2$Mo$_2$(CO)$_4$P$_2$}$_5$]$^{3+}$ (**III**), albeit in minute amounts. In the negative ion ESI-MS spectra of the compounds **3c–g**, only peaks attributable to the corresponding anions are observed.

Owing to the enhanced solubility of **3g**, room temperature positive ion ESI MS spectra of this complex could also be recorded in CH_2Cl_2. The spectra display only one fragment attributable to the monocation **I**. Interestingly, if **1** and Ag[Al{OC(CF$_3$)$_3$}$_4$] are dissolved in CH_2Cl_2 in a 1:1 ratio, **I** is the only fragment containing both Ag^+ cations and units of **1** observed in the ESI MS spectrum of this solution. Furthermore, vapour pressure osmometric (VPO) measurements on **3g** in CH_2Cl_2 at 28 °C suggest the virtually exclusive presence of the monomer [Ag{Cp$_2$Mo$_2$(CO)$_4$P$_2$}$_2$][Al{OC(CF$_3$)$_3$}$_4$] (**7**). The slightly overestimated molecular mass value for **7** (2257 ± 113 g mol^{-1}; calculated: 2067 g mol^{-1}) is indicative of the existence of a small amount of larger species and, therefore, of a monomer/dimer equilibrium, albeit almost exclusively in favour of the monomer.

In order to gain further insight into the structure of the species in solutions of **3g**, variable temperature ^{31}P{^{1}H} NMR spectra were recorded. The spectrum of the compound in CD_2Cl_2 at room temperature displays a slightly broadened singlet at −96.1 ppm, which becomes broader and shifts to lower field as the temperature is reduced, but nevertheless shows no splitting even at −80 °C. ^{31}P NMR measurements on **3g** were thus performed in a 4:1 mixture of [D$_8$]THF and CD_2Cl_2 since it was expected that the splitting of the signal would occur at a temperature below the freezing point of CD_2Cl_2. At room temperature in this mixture, the compound displays a singlet at −82.0 ppm and this signal begins to split at −70 °C. At −80 °C, two peaks are observed, centred at −77.2 and −90.4 ppm, with an integration ratio of approximately 1:2 (Figure 6).

The ^{31}P{^{1}H} NMR spectrum of the gold complex **3h** in CD_2Cl_2 at room temperature exhibits a slightly broadened singlet at −52.7 ppm and a septet at −143.9 ppm (PF_6^-,

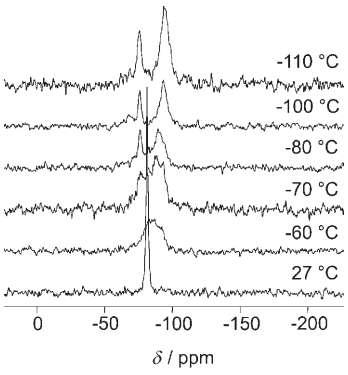

Figure 6. Variable temperature ^{31}P{^{1}H} NMR spectra of **3g** in a 4:1 mixture of [D$_8$]THF and CD_2Cl_2.

$^1J_{PF} = 710$ Hz). In the ESI MS spectra of the compound in CH_2Cl_2, the fragments with the highest relative abundance are attributable to the cations $[Au\{Cp_2Mo_2(CO)_4P_2\}_2(THF)_2]^+$ (THF is present in crystals of **3h**) and $[Au\{Cp_2Mo_2(CO)_4P_2\}_2]^+$. In addition, the fragments detected in the positive ion ESI MS spectra of the reaction solution for the synthesis of **3h** display further peaks attributable to the cations $[Au\{Cp_2Mo_2(CO)_4P_2\}(PPh_3)]^+$ and $[Au(PPh_3)_2]^+$. These data demonstrate, as in the case of the analogous Cu^I and Ag^I complexes, the flexibility of this system and that a monomer/dimer equilibrium most likely exists in solution. In parallel with the observations made for **3g**, which showed that its synthesis appears to be independent of reactant stoichiometry, the reaction of $[(Ph_3P)Au(THF)][PF_6]$ and **1** in a 1:1 stoichiometry also demonstrates this independence and leads to the formation of **3h**.

The solubility of **5** prohibits the acquisition of solution NMR spectra, but the trace amounts of the compound that dissolve in CH_3CN are sufficient for recording ESI MS spectra. Some of the peaks detected in these spectra (for example, $[(Ag_2\{Cp_2Mo_2(CO)_4P_2\}_4)(NO_2)]^+$, $[(Ag_3\{Cp_2Mo_2(CO)_4P_2\}_3)(NO_2)_2]^+$ and $[(Ag_2\{Cp_2Mo_2(CO)_4P_2\}_3)(NO_2)]^+$) demonstrate that species larger than that observed in the solid state structure of **5** are most probably present in solution.

The ^{31}P NMR spectrum of **6** in $[D_8]$THF at room temperature displays a somewhat broadened peak at -77.2 ppm, thus, suggesting dynamic behaviour in solution which may be comparable to that observed for the complex $[\{Cp_2Mo_2(CO)_4(\mu,\eta^2{:}\eta^1\text{-}P_2)\}\{W(CO)_5\}]$.[17] However, this behaviour could not be examined by variable temperature NMR experiments, owing to the poor solubility of **6**. Interestingly, the fragments detected in the positive and negative ion ESI MS spectra of **6** in a mixture of CH_3CN and CH_2Cl_2 suggest that the species in solution might be $[Au\{Cp_2Mo_2(CO)_4P_2\}_2][AuCl_2]$ (**8**).

Theoretical calculations: Density functional theory (DFT) calculations were performed in order to facilitate the interpretation of the spectroscopic data of **3g**. The calculations have shown that the structure of lowest energy for the monocation **I** in CH_2Cl_2 at room temperature is one in which the two units of **1** are bound to the silver cation in a η^2 coordination mode (**Ia**, Scheme 2), and is hence reminiscent of that of the cation $[Ag(\eta^2\text{-}P_4)_2]^+$.[18] It is likely that the structure of the gold-containing monocation in the proposed complex **8** is similar to that of **Ia**.[19]

The monocation **Ia** was calculated to be only 9 kJ mol^{-1} more stable than the $\eta^1{:}\eta^2$ monocation (**Ib**, Scheme 2). The reaction enthalpy for the formation of the dication **II** (Scheme 2) from **Ia** at standard conditions was calculated to be mildly exothermic (-4.5 kJ mol^{-1}), but clearly endergonic (48 kJ mol^{-1}). One could thus envisage the following equilibria in solutions of the compound **3g**: one between the monocations **Ia** and **Ib**, and one between **Ib** and the dication **II** (Scheme 2).

The calculated ^{31}P NMR chemical shifts of the phosphorus atoms in the cations **Ia**, **Ib** and **II** (Scheme 2) are listed in Table 7. The calculated shifts are overestimated compared to the experimental values of **3g** at $-80\,^\circ$C (-77.2, -90.4 ppm). Furthermore, the integration ratio of the signals in the experimental spectrum of **3g** at this temperature ($\approx$1:2) does not correspond to any of those that would be expected for the proposed cations (singlet for **Ia**; 2:1:1 for **Ib**; 1:1 for **II**), which suggests that a mixture of all three cations is most probably present in solutions of **3g**, as might be expected from the small energy differences calculated for these species.

The small positive dissociation enthalpy calculated for the dissociation of dication **II** into **Ia** at standard conditions implies that the concentration of **II** should be higher at lower

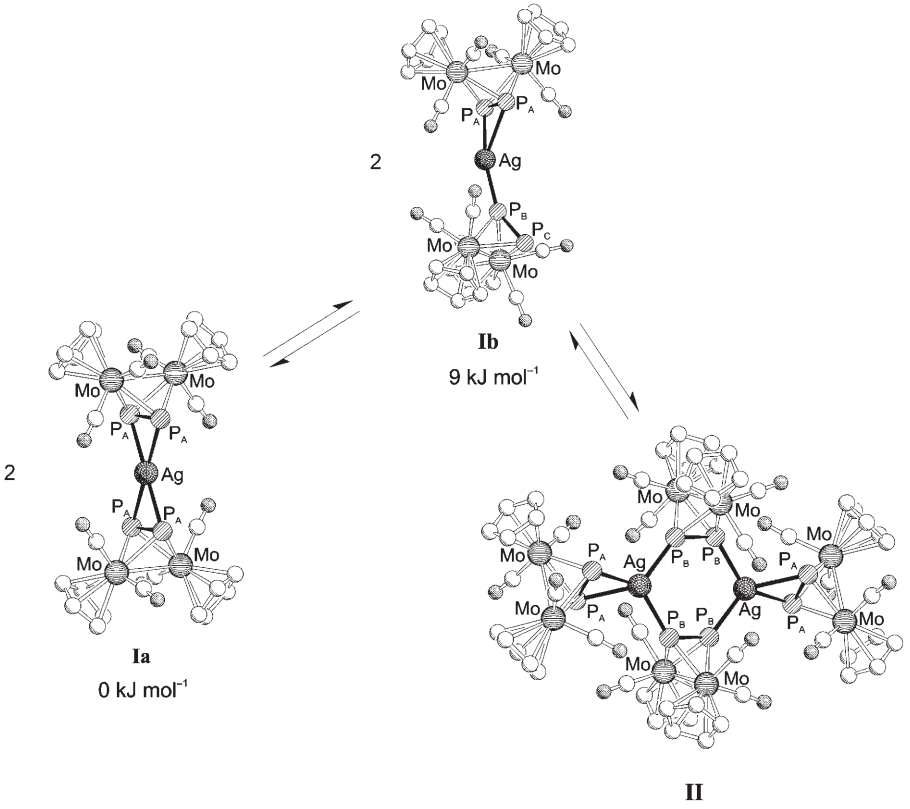

Scheme 2. Proposed equilibria of the cations in solutions of **3g. Ia**, **Ib** and **II** are the calculated cation structures in CH_2Cl_2 at room temperature (hydrogen atoms omitted for clarity).

Table 7. Calculated ^{31}P NMR chemical shifts δ for the cations **Ia**, **Ib** and **II** in CD_2Cl_2 at 0 K (see Scheme 2 for clarification of labelling scheme).

Cation	P atom	δ [ppm]	Average δ [ppm]	δ_{Ia}–Average δ [ppm]
Ia	P_A	−117	–	–
Ib	P_A	−122		
	P_B	−133	−123	6
	P_C	−115		
II	P_A	−124	−140	23
	P_B	−155		

temperatures, since entropic contributions decrease with temperature. Thus, by considering the difference between the ^{31}P NMR chemical shift of the cation **Ia** and the average chemical shifts of the cations **Ib** and **II** (Table 7) as well as the chemical shift difference between the resonances in the experimental spectrum of **3g** at −80 °C (≈13 ppm), the signal at −90.4 ppm in this spectrum may be assigned to the dication **II**. The resonance at −77.2 ppm may then be assigned to the cations **Ia** and **Ib**, which are engaged in a fast exchange process. As the integration ratio of these two signals is approximately 2:1, a monomer:dimer ratio of about 1:1 can be inferred. Furthermore, VPO measurements have demonstrated that room temperature solutions of **3g** consist almost entirely of the monomer **7** and therefore, a monomer concentration of 3 mmol L^{-1} (5 mg of the dimer **3g** in 0.8 mL solvent) can be assumed for the solution under NMR investigation at room temperature. Hence, given that $\Delta_r G = -RT\ln K$, $\Delta_r G$ for the dissociation of **3g** into **7** at −80 °C is about −11 kJ mol^{-1}.

The spectroscopic data of **3g** as well as the solution equilibrium proposed above for the compound (Scheme 2) raise the question of why the dimer **3g**, rather than the monomer **7**, is the species observed in the solid state. The Born–Haber cycle of **3g**, illustrated in Scheme 3, sheds light on this query

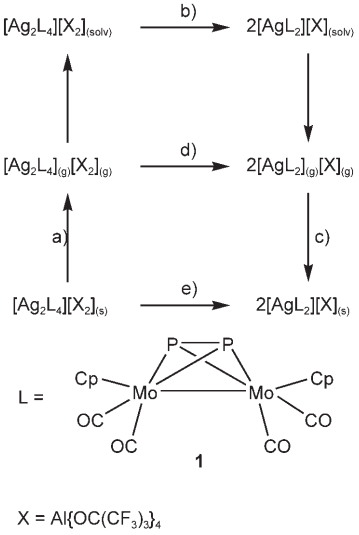

Scheme 3. Born–Haber cycle of **3g**. a) $-\Delta H_{Latt} = 909$ kJ mol^{-1}; b) $\Delta H_{Diss} = 4.5$ kJ mol^{-1} (COSMO/BP86/SV(P)), $\Delta G_{Diss} = -48$ kJ mol^{-1}; c) $\Delta H_{Latt} = -305$ kJ mol^{-1}; d) $\Delta H_{Diss} = -83$ kJ mol^{-1} (BP86/SV(P)); e) $\Delta H_{Diss} = 216$ kJ mol^{-1}.

and demonstrates that crystallisation of the dimer is favoured, owing to the greater lattice energy (−909 kJ mol^{-1} as opposed to −305 kJ mol^{-1} for the monomer **7**), whereas dissolution of **3g** under essentially complete dissociation to **7** is driven by entropy ($\Delta H_{Diss} = 4.5$ kJ mol^{-1}, but $\Delta G_{Diss} = -48$ kJ mol^{-1}).

Solid-state ^{31}P MAS NMR spectra: The inequivalence of the two phosphorus atoms in the new polymorph of **1** (Figure 1) is clearly, if not surprisingly, reflected in its ^{31}P MAS NMR spectrum (Figure 7). The spectrum is characteristic of an

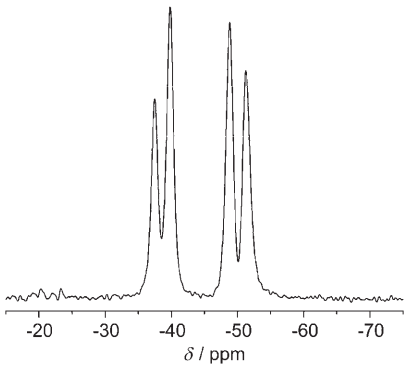

Figure 7. Solid-state ^{31}P MAS NMR spectrum of the new polymorph of **1** at 283.4 MHz and a spinning frequency of 30 kHz.

AB spin system and displays two doublets at −50.0 and −38.6 ppm ($^1J_{PP} = 495 \pm 20$ Hz). In order to assign the resonances, a closer examination of the structural features of the polymorph is necessary. In a previous study in which we analysed the solid state conformation of the polymers **2a-c** (Figure 8) by MAS NMR and DFT calculations,[2d] we showed that subtle differences in the arrangement of the Cp and particularly the CO ligands at the molybdenum atoms have a dramatic effect on the chemical shift of the phosphorus atoms. Thus, the phosphorus atoms within each unit of **1** in the polymers **2a**,**b** have strongly differing chemical shifts, although at first sight, one would expect them to be electronically similar despite being crystallographically distinct. In contrast, only one broad signal is observed in the ^{31}P MAS NMR spectrum of **2c** since the arrangement of the Cp and CO ligands with respect to each phosphorus atom within each unit of **1** is essentially identical.

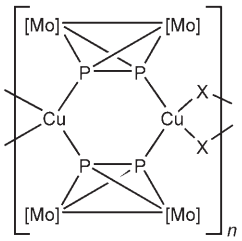

Figure 8. Schematic representation of the structure of the polymers **2a–c**.

An inspection of the average interatomic distance between the CO carbon atoms and the phosphorus atoms within a molecule of **1** in the new polymorph (P1:

3.153(1) Å; P2: 3.165(1) Å) reveals a negligible difference. However, the topologies of the P1 and P2 atoms within a molecule of **1** relative to neighbouring molecules of **1** display noticeable differences, as demonstrated by the structural representations in Figure 9. These representations were

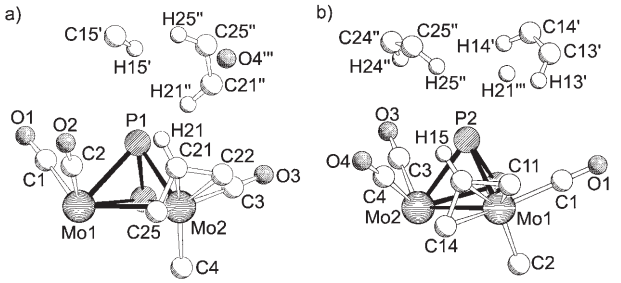

Figure 9. Structural representations demonstrating the differences in the topologies of the a) P1 and the b) P2 atoms in the new polymorph of **1**. In each representation, the relevant phosphorus atom was set as the centre of a sphere with a radius of 4 Å to which all atoms up to 4 Å away from that phosphorus atom were then added.

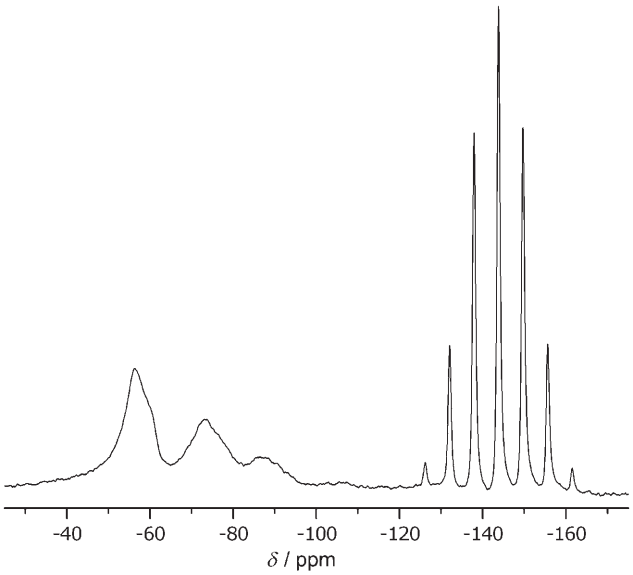

Figure 10. Solid-state ^{31}P MAS NMR spectrum of **3b** at 121.5 MHz and a spinning frequency of 25 kHz.

constructed as follows: the relevant phosphorus atom (P1: Figure 9a; P2: Figure 9a) was set as the centre of a sphere with a radius of 4 Å and then all atoms which were up to 4 Å away from that phosphorus atom were added. The most striking difference in the topologies of the P1 and P2 atoms is the number of Cp carbon atoms (C_{Cp}) of neighbouring molecules of **1** at a distance of less than 4 Å. There are three such atoms in the vicinity of P1 (C15′, C21″, C25″) and four such atoms in the vicinity of P2 (C13′, C14′, C24″, C25″). Furthermore, the average P···C_{Cp} distance (P1: 3.798(1), P2: 3.695(1) Å) is smaller for P2. Thus, the resonance at lower field is tentatively assigned to P2 since the greater number of C_{Cp} atoms of neighbouring molecules of **1** in its vicinity and the shorter average P···C_{Cp} distance, compared to P1, may lead to a somewhat larger deshielding of P2.

The ^{31}P MAS NMR spectrum of the dimer **3b** is depicted in Figure 10. In addition to the septet characteristic of the PF_6^- anion (−143.9 ppm), the spectrum of **3b** exhibits three fairly broad peaks at −89, −74 and −58 ppm with an integrated area ratio of about 1:1:2. Since the structure of **3b** (Figure 11) possesses four types of crystallographically distinct phosphorus atoms (P1–P4), up to four resonances would be expected in the ^{31}P MAS NMR spectrum of **3b**. The coordination of the phosphorus atoms to Cu^I centres might have resulted in multiplet splitting owing to $^{63/65}$Cu dipolar and scalar interactions, but they, however, were not observed.

An inspection of the interatomic distances between the phosphorus atoms of the bridging units of **1** (P1 and P2) and the corresponding CO carbon atoms (C_{CO}; C1–C4) in **3b** suggests that the environments of these two phosphorus atoms are quite similar (Table 8). Likewise, the interatomic

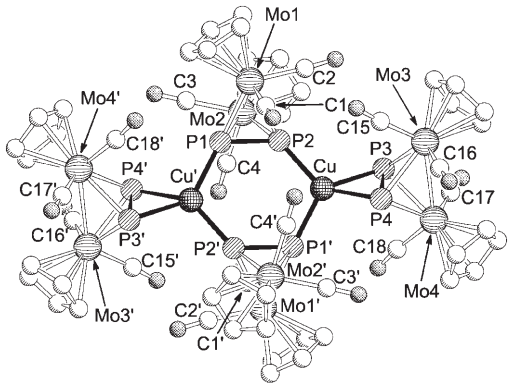

Figure 11. Structure of **3b** (hydrogen atoms omitted for clarity). For selected bond lengths and angles, see Table 4.

distances between the phosphorus atoms of the side-on coordinated units of **1** (P3 and P4) and the corresponding C_{CO} atoms (C15–C18) reveal negligible differences (Table 8). Furthermore, the distances between the P1 and P2 atoms, respectively, and the C_{CO} atoms C1′–C4′, C15–C18 and C15′–C18′ do not exhibit any striking dissimilarities (Table 8). However, an evaluation of the distances between P3 and P4, respectively, and the C_{CO} atoms of the bridging units of **1** (Table 8) shows that P4···C3′ (3.776(2) Å) and P4···C4′ (3.894(2) Å) are particularly short. The shortest P3···C_{CO} distances resulting from this evaluation are P3···C2 (4.576(1) Å) and P3···C4′ (5.408(2) Å). As a consequence of these structural features, P4 is most likely deshielded to a greater extent than P3. Thus, given that the integration ratio of the resonances in the ^{31}P MAS NMR spectrum of **3b** at −89.4, −73.9 and −57.4 ppm is about 1:1:2, the peak at

Table 8. P···C_{CO} interatomic distances [Å] in **3b** (C_{CO} = carbonyl C atom).

P1···C1	3.075(1)	P2···C1	2.985(1)	P3···C1	5.624(2)	P4···C1	5.311(2)
P1···C2	3.906(2)	P2···C2	2.734(1)	P3···C2	4.576(1)	P4···C2	5.330(2)
P1···C3	2.754(1)	P2···C3	3.895(1)	P3···C3	7.369(2)	P4···C3	8.194(2)
P1···C4	2.947(1)	P2···C4	3.183(1)	P3···C4	5.826(2)	P4···C4	6.750(1)
P1···C1′	5.473(2)	P2···C1′	5.411(2)	P3···C1′	6.340(2)	P4···C1′	6.416(1)
P1···C2′	6.228(3)	P2···C2′	6.734(4)	P3···C2′	8.095(4)	P4···C2′	7.456(3)
P1···C3′	6.622(2)	P2···C3′	5.920(3)	P3···C3′	5.436(3)	P4···C3′	3.776(2)
P1···C4′	4.699(1)	P2···C4′	4.407(2)	P3···C4′	5.408(2)	P4···C4′	3.894(2)
P1···C15	5.932(2)	P2···C15	4.253(1)	P3···C15	3.223(1)	P4···C15	2.838(1)
P1···C16	8.114(2)	P2···C16	6.399(1)	P3···C16	3.956(1)	P4···C16	2.780(1)
P1···C17	8.448(3)	P2···C17	6.453(2)	P3···C17	2.749(1)	P4···C17	3.927(1)
P1···C18	7.345(2)	P2···C18	5.693(2)	P3···C18	2.910(1)	P4···C18	3.154(1)
P1···C15′	5.645(2)	P2···C15′	6.910(2)	P3···C15′	9.439(3)	P4···C15′	9.432(3)
P1···C16′	6.339(2)	P2···C16′	7.991(2)	P3···C16′	11.081(3)	P4···C16′	11.325(3)
P1···C17′	6.182(3)	P2···C17′	8.169(3)	P3···C17′	11.595(4)	P4···C17′	11.141(4)
P1···C18′	3.965(2)	P2···C18′	6.003(2)	P3···C18′	9.676(3)	P4···C18′	9.470(3)

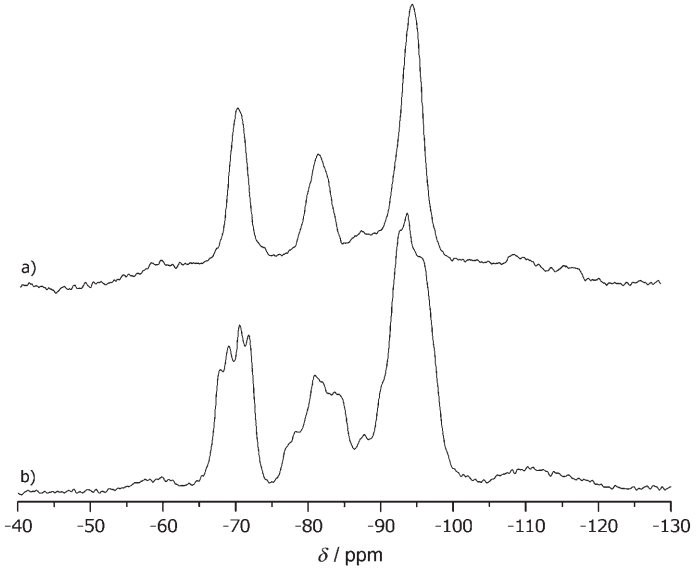

Figure 12. Solid-state ^{31}P MAS NMR spectra of **3c** at a) 283.4 MHz and b) 121.5 MHz, both at a spinning frequency of 30 kHz.

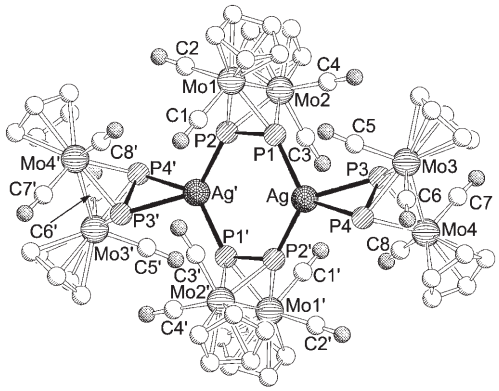

Figure 13. Structure of **3c** (hydrogen atoms omitted for clarity). For selected bond lengths and angles, see Table 4.

−57.4 ppm may be assigned to P1 and P2, because the environments of these two phosphorus atoms are similar. Since P4 is probably more deshielded than P3, the peaks at −89.4 and −73.9 ppm may then be assigned to P3 and P4, respectively.

The solid state ^{31}P MAS NMR spectrum of the dimer **3c** (Figure 12) displays three resonances at −94.3, −81.4 and −69.8 ppm with an integration ratio of approximately 2:1:1. The structure of **3c** (Figure 13) possesses four types of crystallographically distinct P atoms (P1–P4) and hence four resonances would be expected in the ^{31}P MAS NMR spectrum of **3c**, each being flanked by $^{107/109}$Ag satellites. In the experimental spectra, no resolvable couplings to $^{107/109}$Ag are detected, but rather peak splittings, owing to ^{31}P–^{31}P homonuclear *J*-couplings are observed. Examination of the P···C_{CO} interatomic distances in **3c** reveals only minor discrepancies, which are too small to permit an unambiguous assignment of the resonances. However, inspection of the Ag–P bond lengths is more informative. The Ag–P_b bond lengths (Ag–P1 2.487(2), Ag–P2′ 2.468(2) Å) are much shorter than the Ag–P_s bond lengths (Ag–P3 2.699(2), Ag–P4 2.606(2) Å). At the same time, the difference between the Ag–P1 and Ag–P2′ bond lengths is noticeably smaller than that between the Ag–P3 and Ag–P4 bond lengths. Considering the integration ratio of the resonances in the spectrum of **3c**, the peak at −94.3 ppm may therefore be assigned to P1 and P2. In turn, since the Ag–P4 bond length is shorter than that of the Ag–P3 bond, the peaks at −81.4 and −69.8 ppm may then be assigned to P4 and P3, respectively.

The solid-state ^{31}P MAS NMR spectrum of the previously reported 1D polymer **4**[2a] is depicted in Figure 14. It exhibits three resonances at −102.2, −94.1 and −84.7 ppm in an integrated area ratio of approximately 3:2:3 and shows no fine structure, but some peak overlapping is evident. Even an inspection of the relevant P···C_{CO} interatomic distances and Ag–P bond lengths renders an unambiguous assignment of the resonances impossible since six types of crystallographically distinct P atoms are present in the structure of **4** (Figure 15).

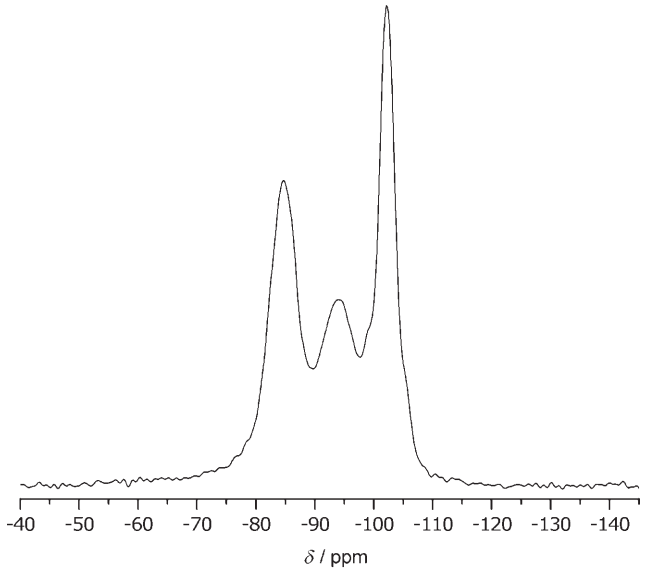

Figure 14. Solid-state ^{31}P MAS NMR spectrum of **4** at 202.5 MHz and a spinning frequency of 30 kHz.

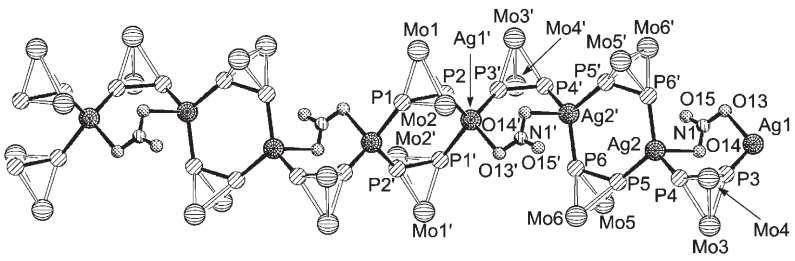

Figure 15. Structure of a section of the polycation in **4** (Cp and CO ligands omitted for clarity).

Conclusion

As compounds **3b–h** demonstrate, reactions of M^I salts of various weakly coordinating anions (WCAs) (M = Cu, Ag, Au) with **1** yield dimeric complex salts consisting of a dication with the same basic structure, regardless of the identity of the WCA. Minor variations of the dication geometry appear to depend on the size of the WCA and hence on crystal packing effects. The compounds **3b–h** appear to exhibit dynamic behaviour in solution, as demonstrated by ^{31}P NMR spectroscopy and ESI-MS. Owing to the excellent solubility characteristics imparted to the dimer **3g** by the $[Al\{OC(CF_3)_3\}_4]^-$ anion, an in-depth investigation of the solution behaviour of this compound could be undertaken. According to VPO measurements, a monomer/dimer equilibrium exists in solutions of **3g**, which is almost exclusively in favour of the monomer at room temperature and shifts in favour of the dimer as the temperature is reduced. DFT calculations support the conclusions drawn from the experimental results.

Solid state ^{31}P MAS NMR measurements were performed on a new polymorph of the starting material **1**, the dimers **3b**,**c** and the previously reported 1D polymer **4**.[2a] Surprisingly, the inequivalence of the P1 and P2 atoms in the new polymorph of **1**, most probably induced by packing effects, is clearly reflected in its spectrum despite the apparently small topological differences. Similarly, the spectra of **3b**,**c** and **4** reveal the extreme sensitivity of the chemical shift to subtle structural differences.

In earlier studies, we showed that reactions of **1** with salts of coordinating anions such as CuX (X = Cl, Br, I)[2a,d] and $AgNO_3$[2a] yield 1D polymers (**2a–c**, **4**) in which all the anions (CuX-based polymers **2a–c**) or one half of the anions ($AgNO_3$-based polymer **4**) are incorporated in the polymer chain. In the light of this observation, experiments were carried out in which the reactivity of **1** with other salts of coordinating anions, namely $AgNO_2$ and LAuCl (L = CO, THT), was probed. Surprisingly, the dimer **5** and the complex **6**, respectively, instead of polymeric products resulted from these reactions, thus demonstrating the versatility of **1** as a ligand.

Experimental Section

General remarks: All manipulations were performed under an atmosphere of dry nitrogen using standard glovebox and Schlenk techniques. All solvents were freshly distilled from appropriate drying agents immediately prior to use. IR spectra were recorded either on a Bruker IFS 280 or a Varian FTS 2000 spectrometer. Solution NMR spectra were acquired either on a Bruker AC250 or a Bruker–Avance 300, 400 or 600 MHz spectrometer. ESI-MS spectra were measured on a Finnigan Thermoquest TSQ 7000 mass-spectrometer. VPO measurements were performed on a Knauer K-7000 vapour pressure osmometer.

Reagents: The compounds **1**,[4b] **4**,[2a] $Ag[Al\{OC(CF_3)_3\}_4]$,[20] $[(Ph_3P)Au(THF)][PF_6]$[10b] and [LAuCl] (L = CO,[5] THT,[6] PPh_3[21]) were prepared according to literature procedures. $[Cu(NCCH_3)_4][PF_6]$ (Aldrich), $[Ag(NCCH_3)_4][BF_4]$ (Aldrich), $AgClO_4$ (Strem), $AgPF_6$ (Aldrich), $AgSbF_6$ (Lancaster), $AgNO_2$ (Fluka) and $TlPF_6$ (Strem) were transferred to a glove-box for storage and used as received.

Crystal structure analysis: Data were collected on an Oxford Gemini R Ultra or a STOE IPDS diffractometer. The structures were solved using either SIR-97[22] or SHELXS-97[23] and refined using SHELXL-97[24] with anisotropic displacements for non-hydrogen atoms. Hydrogen atoms were located in idealised positions and refined isotropically according to the riding model. Only a moderate data set could be collected for compound **6**, since the crystals obtained were of limited quality, despite repeated attempts to crystallise the compound in a variety of solvent systems. CCDC-610584 (**3b**), -610585 (**3c**), -610586 (**3d**), -610587 (**3e**), -610588 (**3f**), -610589 (**3g**), -610590 (**3h**), -610591 (**5**), -610592 (**6**) and -638285 (**1**) contain the supplementary crystallographic data for this paper. These data can be obtained free of charge from the Cambridge Crystallographic Data Centre via www.ccdc.cam.ac.uk/data_request/cif.

Solid state ^{31}P MAS NMR spectroscopy: Solid-state ^{31}P MAS NMR data were obtained at either 283.4 MHz using a Bruker–Avance RX-700 NMR spectrometer or at 202.5 MHz on a Bruker αSX-500 machine. The spectra were recorded using 90° pulses of 2.5 μs and recycle delays of 15–60 s. Additional low-field data were recorded at 121.5 MHz on a Bruker–Avance–II 300 spectrometer. In all cases, a 2.5 mm fast-spinning MAS

probe was employed operating at ambient temperature. All chemical shifts are reported relative to 85% phosphoric acid.

Theoretical calculations: Calculations were executed at the DFT level using the TURBOMOLE programme package.[25] The 28 electron cores of Mo and Ag were replaced by quasi-relativistic effective core potentials.[26] All species were fully optimised using the BP86[27] exchange-correlation functional along with the SV(P) basis set,[28] and solvation energies were calculated using the conductor-like screening model (COSMO) approach.[29] ^{31}P NMR shift calculations, performed at the BP86/SV(P) level (Mo and Ag: SVPalls2 all-electron basis set optimised for NMR calculations),[30] were done as single points on the BP86/SV(P) optimised geometries.

Synthesis of 3b·2 CH_2Cl_2: A solution of $[Cu(NCCH_3)_4][PF_6]$ (37 mg, 0.10 mmol) in CH_2Cl_2 (10 mL) was added to a solution of **1** (100 mg, 0.20 mmol) in CH_2Cl_2 (15 mL). This mixture was kept at room temperature for two days, and red-orange crystals of **3b** were formed. The product was filtered, washed with CH_2Cl_2 (5 mL) and then dried under vacuum. Yield: 106 mg (83%); m.p.: 92°C (decomp.); ^{1}H NMR (300.13 MHz, CD_3CN, 25°C): $\delta = 5.32$ ppm (s; C_5H_5); $^{13}C\{^1H\}$ NMR (100.63 MHz, CD_3CN, 27°C): $\delta = 87.51$ (s; C_5H_5), 226.56 ppm (s; CO); ^{19}F NMR (282.38 MHz, CD_3CN, 25°C): $\delta = -71.67$ ppm (d; $^1J_{PF} = 706$ Hz; $[PF_6^-]$); $^{31}P\{^1H\}$ NMR (121.49 MHz, CD_3CN, 25°C): $\delta = -143.2$ (m; $^1J_{PF} = 706$ Hz; PF_6), −49.6 ppm (s); ^{31}P MAS NMR: $\delta = -89.4$, −73.9, −57.4 ppm; positive ion ESI-MS (CH_3CN, RT): *m/z* (%) = 1099.7 (4) $[Cu\{Cp_2Mo_2(CO)_4P_2\}_2(NCCH_3)]^+$, 1054.8 (42) $[Cu\{Cp_2Mo_2(CO)_4P_2\}_2]^+$, 1028.7 (6) $[Cu\{Cp_2Mo_2(CO)_{3.5}P_2\}_2]^+$, 1002.8 (2) $[Cu\{Cp_2Mo_2(CO)_{1.5}P_2\}_2(NCCH_3)_2]^+$, 985.8 (3) $[Cu\{Cp_2Mo_2(CO)_2P_2\}_2(NCCH_3)]^+$, 957.8 (5) $[Cu\{Cp_2Mo_2(CO)_{1.5}P_2\}_2(NCCH_3)]^+$, 927.8 (1) $[Cu\{Cp_2Mo_2(CO)P_2\}_2(NCCH_3)]^+$, 916.7 (2) $[Cu\{Cp_2Mo_2(CO)_{1.5}P_2\}_2]^+$, 871.8 (2) $[Cu\{Cp_2Mo_2P_2\}_2(NCCH_3)]^+$, 656.1 (2) $[Cu\{Cp_2Mo_2(CO)_3P_2\}(NCCH_3)_3]^+$, 612.8 (6) $[Cu\{Cp_2Mo_2(CO)_3P_2\}(NCCH_3)_2]^+$, 599.9 (28) $[Cu\{Cp_2Mo_2(CO)_4P_2\}(NCCH_3)]^+$, 571.9 (14) $[Cu\{Cp_2Mo_2(CO)_3P_2\}(NCCH_3)]^+$, 543.9 (30) $[Cu\{Cp_2Mo_2(CO)_2P_2\}(NCCH_3)]^+$, 515.9 (14) $[Cu\{Cp_2Mo_2(CO)P_2\}(NCCH_3)]^+$, 145.1 (100) $[Cu(NCCH_3)_2]^+$; negative ion ESI-MS (CH_3CN, RT): *m/z* (%): 145.0 (100) $[PF_6]^-$; IR (KBr): $\tilde{\nu} = 3121$ (w), 1970 (vs; CO), 1936 (vs; CO), 1421 (m), 1358 (w), 1266 (w), 1108 (w), 1065 (m), 1013 (m), 843 (vs), 829 (vs), 733 (m), 702 (w), 558 (s), 520 (m), 489 (m), 455 (s) cm^{-1}; elemental analysis calcd (%) for $C_{29}H_{22}Cl_2CuF_6Mo_4O_8P_5$ (1285.52): C 27.08, H 1.72; found: C 27.07, H 1.71.

Synthesis of 3c: A solution of $[Ag(NCCH_3)_4][BF_4]$ (36 mg, 0.10 mmol) in CH_3CN (25 mL) was added to a solution of **1** (100 mg, 0.20 mmol) in CH_3CN (15 mL) at 0°C. This mixture was kept at −30°C for two days, and red-orange crystals of **3c**·6 CH_3CN were formed. The product was filtered, washed with CH_3CN (15 mL) and then dried under vacuum. The solvent of crystallisation was completely removed during the drying process. Yield: 98 mg (75%); m.p.: 148°C (decomp.); ^{1}H NMR (300.13 MHz, CD_3CN, 25°C): $\delta = 5.31$ ppm (s; C_5H_5); $^{13}C\{^1H\}$ NMR (100.63 MHz, CD_3CN, 27°C): $\delta = 87.43$ (s; C_5H_5), 226.95 ppm (s; CO); ^{19}F NMR (282.38 MHz, CD_3CN, 25°C): $\delta = 150.37$ ppm (s; BF_4^-); $^{31}P\{^1H\}$ NMR (101.26 MHz, CD_3CN, 25°C): $\delta = -71.3$ ppm (s); ^{31}P MAS NMR: −94.3, −81.4, −69.8 ppm; positive ion ESI-MS (CH_3CN, RT): *m/z* (%) = 1207.0 (3) $[Ag_2\{Cp_2Mo_2(CO)_4P_2\}_2]^+$, 1102.8 (2) $[Ag\{Cp_2Mo_2(CO)_4P_2\}_2]^+$, 1056.9 (100) $[Ag\{Cp_2Mo_2(CO)_{2.5}P_2\}_2(NCCH_3)]^+$, 1027.9 (18) $[Ag\{Cp_2Mo_2(CO)_2P_2\}_2(NCCH_3)]^+$, 985.9 (12) $[Ag\{Cp_2Mo_2(CO)_2P_2\}_2]^+$, 957.9 (20) $[Ag\{Cp_2Mo_2(CO)_{1.5}P_2\}_2]^+$, 873.9 (9) $[Ag\{Cp_2Mo_2P_2\}_2]^+$, 745.0 (16) $[Ag_2\{Cp_2Mo_2(CO)_4P_2\}(NCCH_3)]^+$, 602.8 (8) $[Ag\{Cp_2Mo_2(CO)_4P_2\}]^+$; negative ion ESI-MS ($CH_3CN$, RT): *m/z* (%): 87.2 (100) $[BF_4]^-$; IR (KBr): $\tilde{\nu} = 3116$ (w), 1962 (vs; CO), 1930 (vs; CO), 1420 (m), 1358 (w), 1284 (w), 1082 (m), 1048 (m), 1011 (m), 829 (m), 560 (m), 521 (m), 491 (m), 455 (m) cm^{-1}; elemental analysis calcd (%) for $C_{28}H_{20}AgBF_4Mo4O_8P_4$: C 28.31, H 1.68; found: C 28.47, H 1.79.

Synthesis of 3d·2 CH_3CN: A solution of $AgClO_4$ (24 mg, 0.12 mmol) in CH_3CN (10 mL) was carefully layered over a solution of **1** (100 mg, 0.20 mmol) in CH_2Cl_2 (10 mL) at room temperature. The vessel was then placed in a refrigerator (4°C) and red prism-shaped crystals of **3d**·2 CH_3CN appeared within a week. These crystals were filtered, washed with CH_3CN (2×3 mL) and dried under vacuum. Yield: 111 mg (89%); m.p. 160°C (decomp.); ^{1}H NMR (400.13 MHz, CD_3CN, 27°C): $\delta = 5.35$ ppm (s; C_5H_5); $^{13}C\{^1H\}$ NMR (100.63 MHz, CD_3CN, 27°C): $\delta = 87.83$ ppm (s; C_5H_5); $^{31}P\{^1H\}$ NMR (161.98 MHz, CD_3CN, 27°C): $\delta = -59.5$ ppm (s); positive ion ESI-MS (CH_3CN, RT): *m/z* (%) = 2298.9 (1.5) $[(Ag_2\{Cp_2Mo_2(CO)_4P_2\}_4)(ClO_4)]^+$, 1804.9 (1) $[(Ag_2\{Cp_2Mo_2(CO)_4P_2\}_3)(ClO_4)]^+$, 1593.9 (4) $[Ag\{Cp_2Mo_2(CO)_4P_2\}_3]^+$, 1100.8 (100) $[Ag\{Cp_2Mo_2(CO)_4P_2\}_2]^+$, 643.8 (60) $[Ag\{Cp_2Mo_2(CO)_4P_2\}(NCCH_3)]^+$, 597.7 (0.5) $[Ag\{Cp_2Mo_2(CO)_4P_2\}]^+$; negative ion ESI-MS ($CH_3CN$, RT): *m/z* (%): 99.0 (100) $[ClO_4]^-$; IR (KBr): $\tilde{\nu} = 3114$ (w), 1947 (vs; CO), 1919 (vs; CO), 1420 (m), 1104 (s), 1058 (m), 1011 (w), 828 (m), 624 (w), 562 (w), 520 (w), 491 (w), 455 (m) cm^{-1}; elemental analysis calcd (%) for $C_{60}H_{46}Ag_2Cl_2Mo_8N_2O_{24}P_8$ (2480.97): C 29.05, H 1.87, N 1.13; found: C 29.02, H 2.12, N 1.33.

Synthesis of 3e: A mixture of $AgPF_6$ (29 mg, 0.11 mmol), **1** (100 mg, 0.20 mmol) and CH_3CN (30 mL) was stirred in the dark at room temperature for 1 h. The reaction vessel was then placed overnight in a freezer (−28°C), during which time **3e** precipitated as a bright orange microcrystalline powder. The solid was filtered, washed with CH_3CN (2×3 mL) and dried under vacuum. Crystals of **3e**·2 CH_3CN suitable for X-ray diffraction analysis were obtained as red prisms by controlled diffusion of a CH_3CN solution of $AgPF_6$ into a CH_2Cl_2 solution of **1** at room temperature in the absence of light. Yield: 70 mg (56%); m.p.: 180°C (decomp.); ^{1}H NMR (600.13 MHz, CD_3CN, 27°C): $\delta = 5.38$ ppm (s; C_5H_5); $^{13}C\{^1H\}$ NMR (150.92 MHz, CD_3CN, 27°C): $\delta = 88.45$ (s; C_5H_5), 226.22 ppm (s; CO); ^{19}F NMR (376.47 MHz, CD_3CN, 27°C): $\delta = -71.74$ ppm (d; $^1J_{PF} = 706$ Hz; $[PF_6^-]$); $^{31}P\{^1H\}$ NMR (161.98 MHz, CD_3CN,27°C): $\delta = -143.1$ (m; $^1J_{PF} = 706$ Hz; PF_6), −64.2 ppm (s); positive ion ESI-MS (CH_3CN, RT): *m/z* (%): 3095.2 (0.1) $[(Ag_3\{Cp_2Mo_2(CO)_4P_2\}_5)(PF_6)_2]^+$, 2346.8 (1) $[(Ag_2\{Cp_2Mo_2(CO)_4P_2\}_4)(PF_6)]^+$, 2100.7 (0.5) $[(Ag_3\{Cp_2Mo_2(CO)_4P_2\}_3)(PF_6)_2]^+$, 1847.6 (0.5) $[(Ag_2\{Cp_2Mo_2(CO)_4P_2\}_3)(PF_6)]^+$, 1595.0 (10) $[Ag\{Cp_2Mo_2(CO)_4P_2\}_3]^+$, 1100.7 (100) $[Ag\{Cp_2Mo_2(CO)_4P_2\}_2]^+$, 645.8 (60) $[Ag\{Cp_2Mo_2(CO)_4P_2\}(NCCH_3)]^+$, 600.7 (8) $[Ag\{Cp_2Mo_2(CO)_4P_2\}]^+$; negative ion ESI-MS ($CH_3CN$, RT): *m/z* (%): 145.0 (100) $[PF_6]^-$; IR (KBr): $\tilde{\nu} = 2926$ (w), 1953 (vs; CO), 1915 (vs; CO), 1420 (m), 1108 (w), 1063 (w), 1012 (w), 868 (s), 846 (s), 831 (s), 558 (m), 530 (m), 520 (m), 493 (w), 457 (m), 442 (m) cm^{-1}; elemental analysis calcd (%) for $C_{56}H_{40}Ag_2F_{12}Mo_8O_{16}P_{10}$ (2489.90): C 27.01, H 1.62; found: C 27.25, H 1.58.

Synthesis of 3f: A mixture of $AgSbF_6$ (40 mg, 0.12 mmol), **1** (100 mg, 0.20 mmol) and CH_3CN (30 mL) was stirred in the absence of light at room temperature for 1 h. The reaction vessel was then placed overnight in a freezer (−28°C), during which time **3f** precipitated as a bright orange microcrystalline powder. The solid was filtered, washed with CH_3CN (2×3 mL) and dried under vacuum. Crystals of **3f**·4.5 CH_3CN suitable for X-ray diffraction analysis were obtained as orange-red prisms by controlled diffusion of a CH_3CN solution of $AgSbF_6$ into a CH_2Cl_2 solution of **1** at room temperature in the dark. Yield: 85 mg (63%); m.p.: 170°C (decomp.); ^{1}H NMR (400.13 MHz, CD_3CN, 27°C): $\delta = 5.34$ ppm (s; C_5H_5); $^{13}C\{^1H\}$ NMR (100.63 MHz, CD_3CN, 27°C): $\delta = 88.06$ (s; C_5H_5), 225.08 ppm (s; CO); ^{19}F NMR (CD_3CN, 376.47 MHz, 27°C): $\delta = -122.82$ (m; $^1J_{SbF} = 1050$ Hz; $^{123}SbF_6^-$), −122.81 ppm (m; $^1J_{SbF} = 1934$ Hz; $^{121}SbF_6^-$); $^{31}P\{^1H\}$ NMR (161.98 MHz, CD_3CN, 27°C): $\delta = -71.3$ ppm (s); positive ion ESI-MS (CH_3CN, RT): *m/z* (%): 2436.9 (2) $[(Ag_2\{Cp_2Mo_2(CO)_4P_2\}_4)(SbF_6)]^+$, 1941.1 (0.5) $[(Ag_2\{Cp_2Mo_2(CO)_4P_2\}_3)(SbF_6)]^+$, 1596.7 (4) $[Ag\{Cp_2Mo_2(CO)_4P_2\}_3]^+$, 1100.8 (100) $[Ag\{Cp_2Mo_2(CO)_4P_2\}_2]^+$, 643.9 (30) $[Ag\{Cp_2Mo_2(CO)_4P_2\}(NCCH_3)]^+$, 601.9 (0.5) $[Ag\{Cp_2Mo_2(CO)_4P_2\}]^+$; negative ion ESI-MS ($CH_3CN$, RT): *m/z* (%): 234.8 (100) $[SbF_6]^-$; IR (KBr): $\tilde{\nu} = 3121$ (w), 1965 (vs; CO), 1946 (vs; CO), 1422 (m), 1109 (w), 1063 (w), 1012 (w), 837 (m), 829 (m), 660 (s), 560 (m), 519 (m), 490 (m), 456 (m) cm^{-1}; elemental analysis calcd (%) for $C_{56}H_{40}Ag_2F_{12}Mo_8O_{16}P_8Sb_2$ (2671.45): C 25.18, H 1.51; found: C 25.17, H 1.68.

Synthesis of 3g: A mixture of $Ag[Al\{OC(CF_3)_3\}_4]$·CH_2Cl_2 (117 mg, 0.10 mmol), **1** (100 mg, 0.20 mmol) and CH_2Cl_2 (10 mL) was stirred in the absence of light for 8 h at room temperature. The solution was filtered over diatomaceous earth, which was subsequently washed with CH_2Cl_2 (2×2 mL). The combined filtrate and washings were stored in a freezer (−28°C) and crystals of **3g**·CH_2Cl_2 appeared within two days in the form

of orange-red needles. These crystals were isolated by filtration at −30 °C, washed with pentane (2×3 mL) at room temperature and dried under vacuum. The solvent of crystallisation was completely removed during the drying process. Addition of an equal volume of pentane to the mother liquor led to the isolation of a further crop of **3g** as a bright orange powder. Alternatively, **3g**·CH_2Cl_2 can be prepared in the form of red prisms by controlled diffusion of a toluene solution of **1** into a CH_2Cl_2 solution of $Ag[Al\{OC(CF_3)_3\}_4]$ at room temperature in the absence of light. Yield: 168 mg (81 %); m.p.: 179 °C (decomp.); ^{1}H NMR (400.13 MHz, CD_2Cl_2, 27 °C): δ = 5.36 ppm (s; C_5H_5); $^{13}C\{^1H\}$ NMR (62.90 MHz, CD_2Cl_2, 27 °C): δ = 87.81 (s; C_5H_5), 121.66 (q; $^1J_{FC}$ = 291 Hz; CF_3), 223.09 ppm (s; CO); ^{27}Al NMR (78.21 MHz, CD_2Cl_2, 27 °C): δ = 33.77 ppm (s; $[Al\{OC(CF_3)_3\}_4]^-$); ^{19}F NMR (376.50 MHz, CD_2Cl_2, 25 °C): δ = −75.32 ppm (s; CF_3); $^{31}P\{^1H\}$ NMR (161.98 MHz, CD_2Cl_2, 27 °C): δ = −96.1 ppm (s); $^{31}P\{^1H\}$ NMR (161.98 MHz, CD_3CN, 27 °C): δ = −77.5 ppm (s); $^{31}P\{^1H\}$ NMR ($[D_8]$THF/CD_2Cl_2 (4:1), 161.98 MHz, 27 °C): δ = −82.0 ppm (s); $^{31}P\{^1H\}$ NMR ($[D_8]$THF/CD_2Cl_2 (4:1), 161.98 MHz, −110 °C): δ = −95.2 (b), −77.3 ppm (b); positive ion ESI-MS (CH_2Cl_2, RT): *m/z* (%): 1100.8 (100) $[Ag\{Cp_2Mo_2(CO)_4P_2\}_2]^+$; negative ion ESI-MS ($CH_2Cl_2$, RT): *m/z* (%): 967.1 (100) $[Al\{OC(CF_3)_3\}_4]^-$; positive ion ESI-MS (CH_3CN, RT): *m/z* (%): 3164.2 (45) $[(Ag_2\{Cp_2Mo_2(CO)_4P_2\}_4)(Al\{OC(CF_3)_3\}_4)]^+$, 2670.6 (3.5) $[(Ag_2\{Cp_2Mo_2(CO)_4P_2\}_3)(Al\{OC(CF_3)_3\}_4)]^+$, 1100.7 (100) $[Ag\{Cp_2Mo_2(CO)_4P_2\}_2]^+$, 643.8 (35) $[Ag\{Cp_2Mo_2(CO)_4P_2\}(NCCH_3)]^+$; negative ion ESI-MS ($CH_3CN$, RT): *m/z* (%): 967.1 (100) $[Al\{OC(CF_3)_3\}_4]^-$; IR (CH_2Cl_2): $\tilde{\nu}$ = 1987 (s; CO), 1943 (s; CO), 1420 (w), 1352 (m), 1300 (s), 1278 (s), 1264 (s), 1241 (vs), 1224 (vs), 976 (vs) cm^{-1}; IR (KBr): ν bar = 1985 (vs; CO), 1951 (vs; CO), 1423 (m), 1352 (s), 1302 (vs), 1277 (vs), 1242 (vs), 1219 (vs), 1169 (m), 1066 (w), 1014 (w), 974 (vs), 829 (s), 756 (w), 728 (vs), 561 (m), 537 (m), 520 (m), 488 (m), 444 (s) cm^{-1}; theoretical molecular mass for $C_{88}H_{40}Ag_2Al_2F_{72}Mo_8O_{24}P_8$: 4134.17 g mol^{-1}; found (osmometric, CH_2Cl_2, 28 °C): 2257 ± 113 g mol^{-1}; elemental analysis calcd (%) for $C_{88}H_{40}Ag_2Al_2F_{72}Mo_8O_{24}P_8$ (4134.17): C 25.57, H 0.98; found: C 25.72, H 1.04.

Synthesis of 3h·2 C_4H_8O·2 CH_2Cl_2: A mixture of $[(Ph_3P)AuCl]$ (46 mg, 0.09 mmol), $TlPF_6$ (35 mg, 0.10 mmol), THF (5 mL) and CH_2Cl_2 (5 mL) was stirred at room temperature in the dark for 8 h, during which time TlCl was formed as a fine pale grey precipitate. The $[(Ph_3P)Au(THF)][PF_6]$ solution was filtered over diatomaceous earth, which was subsequently washed with THF (2×2 mL). The combined filtrate and washings were added to a solution of **1** (100 mg, 0.20 mmol) in CH_2Cl_2 (10 mL). This mixture was stirred overnight and then filtered over diatomaceous earth, which was subsequently washed with CH_2Cl_2 (2×3 mL). The combined filtrate and washings were concentrated under reduced pressure and at room temperature to about a quarter of the original volume and stored at −28 °C. Ruby red plates of **3h**·2 C_4H_8O·2 CH_2Cl_2 crystallised within a week and were filtered, washed with pentane (2×3 mL) and dried under vacuum. Yield: 45 mg (32 %); m.p.: 166 °C (decomp.); ^{1}H NMR (400.13 MHz, CD_2Cl_2, 27 °C): δ = 1.82 (m; THF), 3.68 (m; THF), 5.39 ppm (s; C_5H_5); $^{13}C\{^1H\}$ NMR (CD_2Cl_2, 100.63 MHz, 27 °C): δ = 25.99 (s; THF), 68.18 (s; THF), 88.45 (s; C_5H_5), 222.67 ppm (s; CO); ^{19}F NMR (376.47 MHz, CD_2Cl_2, 27 °C): δ = −73.35 ppm (d; $^1J_{PF}$ = 710 Hz; $[PF_6^-]$); $^{31}P\{^1H\}$ NMR (161.98 MHz, CD_2Cl_2, 27 °C): δ = −143.9 (m; $^1J_{PF}$ = 710 Hz; $[PF_6^-]$), −52.7 ppm (s); positive ion ESI-MS (CH_2Cl_2, RT): *m/z* (%): 1340.5 (100) $[Au\{Cp_2Mo_2(CO)_4P_2\}_2(THF)_2]^+$, 1190.8 (98) $[Au\{Cp_2Mo_2(CO)_4P_2\}_2]^+$, 1161.7 (15) $[Au\{Cp_2Mo_2(CO)_{3.5}P_2\}_2]^+$, 1134.7 (94) $[Au\{Cp_2Mo_2(CO)_3P_2\}_2]^+$, 1105.7 (100) $[(Au_2\{Cp_2Mo_2(CO)_4P_2\}\{THF\})(PF_6)]^+$, 1077.8 (6) $[(Au_2\{Cp_2Mo_2(CO)_3P_2\}\{THF\})(PF_6)]^+$, 1048.6 (4) $[(Au_2\{Cp_2Mo_2(CO)_2P_2\}(THF))(PF_6)]^+$; negative ion ESI-MS ($CH_2Cl_2$, RT): *m/z* (%): 144.9 (100) $[PF_6]^-$; IR (KBr): $\tilde{\nu}$ = 1975 (vs; CO), 1942 (vs; CO), 1637 (m), 1559 (m), 1420 (m), 1357 (w), 1262 (w), 1063 (w), 1012 (w), 845 (s), 830 (s), 668 (m), 558 (s), 518 (m), 488 (m), 456 (m) cm^{-1}; elemental analysis calcd (%) for $C_{66}H_{60}Au_2Cl_4F_{12}Mo_8O_{18}P_{10}$ (2982.17): C 26.58, H 2.03; found: C 26.74, H 1.98.

Synthesis of 5: A mixture of $AgNO_2$ (35 mg, 0.23 mmol), **1** (100 mg, 0.20 mmol) and CH_3CN (30 mL) was stirred in the absence of light at room temperature for 1 h, during which time **5** was formed as a microcrystalline dark brown powder. The solid was filtered, washed with CH_3CN (2×3 mL) and dried under vacuum. Crystals of **5** suitable for X-ray diffraction analysis were obtained as dark brown plates by controlled diffusion of a CH_3CN solution of $AgNO_2$ into a CH_2Cl_2 solution of **1** at room temperature in the dark. Yield: 121 mg (92 %); m.p.: 103 °C (decomp.); positive ion ESI-MS (CH_3CN, RT): *m/z* (%): 2249.8 (8) $[(Ag_2\{Cp_2Mo_2(CO)_4P_2\}_4)(NO_2)]^+$, 1904.7 (20) $[(Ag_3\{Cp_2Mo_2(CO)_4P_2\}_3)(NO_2)_2]^+$, 1748.9 (38) $[(Ag_2\{Cp_2Mo_2(CO)_4P_2\}_3)(NO_2)]^+$, 1596.8 (11) $[Ag\{Cp_2Mo_2(CO)_4P_2\}_3]^+$, 1255.8 (5) $[(Ag_2\{Cp_2Mo_2(CO)_4P_2\}_2)(NO_2)]^+$, 1100.7 (100) $[Ag\{Cp_2Mo_2(CO)_4P_2\}_2]^+$, 643.8 (40) $[Ag\{Cp_2Mo_2(CO)_4P_2\}(NCCH_3)]^+$, 599.9 (1) $[Ag\{Cp_2Mo_2(CO)_4P_2\}]^+$; negative ion ESI-MS ($CH_3CN$, RT): *m/z* (%): 46.3 (100) $[NO_2]^-$; IR (KBr): $\tilde{\nu}$ = 3115 (w), 1997 (vs; CO), 1954 (vs; CO), 1919 (vs; CO), 1419 (m), 1264 (m), 1241 (m), 1103 (w), 1061 (w), 1010 (w), 867 (w), 828 (m), 669 (w), 559 (w), 514 (w), 483 (w), 455 (m) cm^{-1}; elemental analysis calcd (%) for $C_{28}H_{20}Ag_2Mo_4N_2O_{12}P_4$ (1299.86): C 25.87, H 1.55, N 2.16; found: C 25.41, H 1.83, N 2.07.

Synthesis of 6: A room temperature solution of **1** (100 mg, 0.20 mmol) in toluene (10 mL) was layered over a frozen solution of [(OC)AuCl] (52 mg, 0.20 mmol) in toluene (10 mL) submerged in a Dewar flask containing liquid nitrogen. The vessel was left in the Dewar flask, connected to a mercury valve, and allowed to gradually reach room temperature in the absence of light. Crystals of **6** were formed within two weeks as red needles, which were filtered, washed with pentane (2×3 mL) and dried under vacuum. Alternatively, **6** can be prepared as an orange powder by mixing [(THT)AuCl] and **1** in CH_2Cl_2 at room temperature. Yield: 130 mg (89 %); m.p.: 160 °C (decomp.); ^{1}H NMR (400.13 MHz, $[D_8]$THF, 27 °C): δ = 5.55 ppm (s; C_5H_5); $^{31}P\{^1H\}$ NMR ($[D_8]$THF, 161.98 MHz, 27 °C): δ = −77.2 ppm (b); positive ion ESI-MS (CH_3CN/CH_2Cl_2, RT): *m/z* (%): 1915.0 (2.5) $[Au_2Cl\{Cp_2Mo_2(CO)_4P_2\}_3]^+$, 1425.0 (1.5) $[Au_2Cl\{Cp_2Mo_2(CO)_4P_2\}_2]^+$, 1189.0 (100) $[Au\{Cp_2Mo_2(CO)_4P_2\}_2]^+$; negative ion ESI-MS ($CH_3CN/CH_2Cl_2$, RT):
m/z (%): 996.9 (2.5) $[Au_2Cl_3\{Cp_2Mo_2(CO)_4P_2\}]^-$, 266.8 (100) $[AuCl_2]^-$; IR (KBr): $\tilde{\nu}$ = 3098 (w), 2006 (vs; CO), 1984 (vs; CO), 1946 (vs; CO), 1924 (vs; CO), 1630 (w), 1418 (m), 1356 (w), 1263 (w), 1105 (w), 1060 (w), 928 (w), 854 (w), 839 (m), 829 (m), 818 (m), 735 (w), 605 (w), 561 (m), 519 (s), 485 (m), 456 (s), 447 (s) cm^{-1}; elemental analysis calcd (%) for $C_{14}H_{10}AuClMo_2O_4P_2$ (728.48): C 23.08, H 1.38; found: C 22.65, H 1.43.

Acknowledgements

This work was comprehensively supported by the Deutsche Forschungsgemeinschaft and the Fonds der Chemischen Industrie. The authors would like to thank Prof. Werner Kunz and Dr. Roland Neueder for providing the VPO equipment, Mrs. Petra Lugauer and Mrs. Sabine Stempfhuber for technical assistance, and Umicore AG for the gift of precious metals.

[1] Recent review articles: a) W. Huang, H.-B. Zhu, S.-H. Gou, *Coord. Chem. Rev.* **2006**, *250*, 414–423; b) N. C. Gianneschi, M. S. Masar III, C. A. Mirkin, *Acc. Chem. Res.* **2005**, *38*, 825–837; c) M. Ruben, J. Rojo, F. J. Romero-Salguero, L. H. Uppadine, J. -M. Lehn, *Angew. Chem.* **2004**, *116*, 3728–3747; *Angew. Chem. Int. Ed.* **2004**, *43*, 3644–3662; d) L. Carlucci, G. Ciani, D. M. Proserpio, *Coord. Chem. Rev.* **2003**, *246*, 247–289; e) G. F. Swiegers, T. J. Malefetse, *Coord. Chem. Rev.* **2002**, *225*, 91–121.

[2] a) J. Bai, E. Leiner, M. Scheer, *Angew. Chem.* **2002**, *114*, 820–823; *Angew. Chem. Int. Ed.* **2002**, *41*, 783–786; b) J. Bai, A. V. Virovets, M. Scheer, *Angew. Chem.* **2002**, *114*, 1808–1811; *Angew. Chem. Int. Ed.* **2002**, *41*, 1737–1740; c) J. Bai, A. V. Virovets, M. Scheer, *Science* **2003**, *300*, 781–783; d) M. Scheer, L. Gregoriades, J. Bai, M. Sierka, G. Brunklaus, H. Eckert, *Chem. Eur. J.* **2005**, *11*, 2163–2169; e) M. Scheer, J. Bai, B. P. Johnson, R. Merkle, A. V. Virovets, C. E. Anson, *Eur. J. Inorg. Chem.* **2005**, 4023–4026; f) B. P. Johnson, F. Dielmann, G. Balázs, M. Sierka, M. Scheer, *Angew. Chem.* **2006**, *118*, 2533–2536; *Angew. Chem. Int. Ed.* **2006**, *45*, 2473–2475; g) L. J. Gregoriades, H. Krauss, J. Wachter, A. V. Virovets, M. Sierka, M. Scheer, *Angew. Chem.* **2006**, *118*, 4295–4298; *Angew. Chem. Int. Ed.*

2006, *45*, 4189–4192; h) M. Scheer, L. J. Gregoriades, A. V. Virovets, W. Kunz, R. Neueder, I. Krossing, *Angew. Chem.* **2006**, *118*, 5818–5822; *Angew. Chem. Int. Ed.* **2006**, *45*, 5689–5693; i) M. Scheer, L. J. Gregoriades, M. Zabel, M. Sierka, L. Zhang, H. Eckert, *Eur. J. Inorg. Chem.* **2007**, 2775–2782.

[3] a) M. Pronold, M. Scheer, J. Wachter, M. Zabel, *Inorg. Chem.* **2007**, *46*, 1396–1400; b) L. J. Gregoriades, G. Balázs, E. Brunner, C. Gröger, J. Wachter, M. Zabel, M. Scheer, *Angew. Chem.* **2007**, *119*, 6070–6074; *Angew. Chem. Int. Ed.* **2007**, *46*, 5966–5970.

[4] a) O. J. Scherer, H. Sitzmann, G. Wolmershäuser, *J. Organomet. Chem.* **1984**, *268*, C9-C12; b) O. J. Scherer, J. Schwalb, H. Sitzmann, *Inorg. Synth.* **1990**, *27*, 224–227.

[5] D. Belli Dell′Amico, F. Calderazzo, *Inorg. Synth.* **1986**, *24*, 236–238.

[6] R. Uson, A. Laguna, M. Laguna, *Inorg. Synth.* **1989**, *26*, 85–91.

[7] This work.

[8] a) L. M. Engelhardt, C. Pakawatchai, A. H. White, P. C. Healy, *J. Chem. Soc. Dalton Trans.* **1985**, 125–133; b) G. A. Bowmaker, P. C. Healy, L. M. Engelhardt, J. D. Kildea, B. W. Skelton, A. H. White, *Aust. J. Chem.* **1990**, *43*, 1697–1705.

[9] a) C. Pelizzi, G. Pelizzi, P. Tarasconi, *J. Organomet. Chem.* **1984**, *277*, 29–35; b) P. F. Barron, J. C. Dyason, P. C. Healy, L. M. Engelhardt, B. W. Skelton, A. H. White, *J. Chem. Soc. Dalton Trans.* **1986**, 1965–1970; c) F. A. Cotton, R. L. Luck, *Acta Cryst. Sect. A Acta Cryst.* **1989**, *C45*, 1222–1224; d) D. D. Ellis, A. L. Spek, *Acta Cryst. Sect. A* **2000**, *C56*, e547-e548.

[10] a) M. Di Vaira, M. P. Ehses, M. Peruzzini, P. Stoppioni, *Polyhedron* **1999**, *18*, 2331–2336; b) M. Di Vaira, P. Stoppioni, M. Peruzzini, *J. Chem. Soc. Dalton Trans.* **1990**, 109–113.

[11] P. G. Jones, *J. Chem. Soc. Chem. Commun.* **1980**, 1031–1033 ([Au(PPh_3)$_4$][BPh_4] can be crystallised in three modifications (**I**, **II** and **III**). In **I**, the Au atom is actually in a trigonal coordination mode since the Au···P contact with the fourth PPh_3 ligand is markedly longer (3.946 Å). In **II** and **III**, the Au atoms are found in both trigonal and tetrahedral coordination environments. The range quoted is defined by the Au–P bond lengths found in all three modifications, excluding the aforementioned long contact.).

[12] P. A. Bates, J. M. Waters, *Inorg. Chim. Acta* **1984**, *81*, 151–156.

[13] a) H. K. Roobottom, H. D. B. Jenkins, J. Passmore, L. Glasser, *J. Chem. Educ.* **1999**, *76*, 1570–1573; b) I. Krossing, H. Brands, R. Feuerhake, S. Koenig, *J. Fluorine Chem.* **2001**, *112*, 83–90.

[14] Effendy, J. V. Hanna, F. Marchetti, D. Martini, C. Pettinari, R. Pettinari, B. W. Skelton, A. H. White, *Inorg. Chim. Acta* **2004**, *357*, 1523–1537.

[15] N. C. Baenziger, W. E. Bennett, D. M. Soboroff, *Acta Cryst.* **1976**, *B32*, 962–963.

[16] Compounds **3e**,**h** also display septets at approximately −145 ppm, owing to the [PF_6^-] ion.

[17] M. Scheer, E. Leiner, P. Kramkowski, M. Schiffer, G. Baum, *Chem. Eur. J.* **1998**, *4*, 1917–1923.

[18] a) I. Krossing, *J. Am. Chem. Soc.* **2001**, *123*, 4603–4604; b) I. Krossing, L. van Wüllen, *Chem. Eur. J.* **2002**, *8*, 700–711; c) A. Bihlmeier, M. Gonsior, I. Raabe, N. Trapp, I. Krossing, *Chem. Eur. J.* **2004**, *10*, 5041–5051.

[19] H. -C. Tai, C. Lim, I. Krossing, M. Seth, D. V. Deubel, *Organometallics* **2004**, *23*, 2343–2349.

[20] I. Krossing, *Chem. Eur. J.* **2001**, *7*, 490–502.

[21] P. Braunstein, H. Lehner, D. Matt, *Inorg. Synth.* **1990**, *27*, 218–221.

[22] A. Altomare, G. Cascarano, C. Giacovazzo, A. Guagliardi, *J. Appl. Crystallogr.* **1993**, *26*, 343–350.

[23] G. M. Sheldrick, *SHELXS-97*, University of Göttingen, **1997**.

[24] G. M. Sheldrick, *SHELXL-97*, University of Göttingen, **1997**.

[25] a) R. Ahlrichs, M. Bär, M. Häser, H. Horn, C. Kölmel, *Chem. Phys. Lett.* **1989**, *162*, 165–169; b) O. Treutler, R. Ahlrichs, *J. Chem. Phys.* **1995**, *102*, 346–354.

[26] W. Küchle, M. Dolg, H. Stoll, H. Preuss, *Mol. Phys.* **1991**, *74*, 1245–1263.

[27] a) A. D. Becke, *Phys. Rev. A* **1988**, *38*, 3098–3100; b) S. H. Vosko, L. Wilk, M. Nusair, *Can. J. Phys.* **1980**, *58*, 1200–1211; c) J. P. Perdew, *Phys. Rev. B* **1986**, *33*, 8822–8824; d) J. P. Perdew, *Phys. Rev. B* **1986**, *34*, 7406.

[28] K. Eichkorn, O. Treutler, H. Öhm, M. Häser, R. Ahlrichs, *Chem. Phys. Lett.* **1995**, *242*, 652–660.

[29] A. Klamt, G. Schüürmann, *J. Chem. Soc. Perkin. Trans.* **1993**, *2*, 799–805.

[30] a) A. Schäfer, H. Horn, R. Ahlrichs, *J. Chem. Phys.* **1992**, *97*, 2571–2577; b) A. Schäfer, C. Huber, R. Ahlrichs, *J. Chem. Phys.* **1994**, *100*, 5829–5835.

Received: May 10, 2007
Published online: September 26, 2007

